frontiers | Frontiers in Chemical Biology

TYPE Original Research
PUBLISHED 12 August 2024
DOI 10.3389/fchbi.2024.1451167

OPEN ACCESS

EDITED BY
Debbie C. Crans,
Colorado State University, United States

REVIEWED BY
Haiyan Fan,
Nazarbayev University, Kazakhstan
Nadiia I. Gumerova,
University of Vienna, Austria
Manuel Aureliano,
University of Algarve, Portugal

*CORRESPONDENCE
María Eugenia Castro,
mareug.castro@correo.buap.mx
Enrique González-Vergara,
enrique.gonzalez@correo.buap.mx

RECEIVED 18 June 2024
ACCEPTED 16 July 2024
PUBLISHED 12 August 2024

CITATION
Paredes-Pérez LF, Mendoza A, García-García A, Serrano-De la Rosa LE, Méndez-Rojas MA, Melendez FJ, Castro ME and González-Vergara E (2024), Guanidinium and spermidinium decavanadates: as small biomimetic models to understand non-covalent interactions between decavanadate and arginine and lysine side chains in proteins. *Front. Chem. Biol* 3:1451167.
doi: 10.3389/fchbi.2024.1451167

Guanidinium and spermidinium decavanadates: as small biomimetic models to understand non-covalent interactions between decavanadate and arginine and lysine side chains in proteins

Luis F. Paredes-Pérez[1], Angel Mendoza[1], Amalia García-García[2], Laura E. Serrano-De la Rosa[3], Miguel A. Méndez-Rojas[4], Francisco J. Melendez[5], María Eugenia Castro[1]* and Enrique González-Vergara[1]*

[1]Centro de Química del Instituto de Ciencias, Benemérita Universidad Autónoma de Puebla, Puebla, Mexico, [2]Departamento de Química Inorgánica, Facultad de Ciencias, Universidad de Granada, Granada, Spain, [3]Laboratorio Central del Instituto de Física "Luis Rivera Terrazas" (IFUAP), Benemérita Universidad Autónoma de Puebla, Puebla, Mexico, [4]Departamento de Ciencias Químico-Biológicas, Universidad de las Américas, Puebla, Mexico, [5]Facultad de Ciencias Químicas, Benemérita Universidad Autónoma de Puebla, Puebla, Mexico

During the last three decades, numerous investigations have been conducted on polyoxidovanadates to treat several illnesses and inhibit enzymes. Numerous decavanadate compounds have been proposed as potential therapies for Diabetes mellitus, Cancer, and Alzheimer's disease. Only six relevant functional proteins interacting with decavanadate, V_{10}, have been deposited in the PDB. These are acid phosphatase, tyrosine kinase, two ecto-nucleoside triphosphate diphosphohydrolases (NTPDases), the human transient receptor potential cation channel (TRPM4), and the human cell cycle protein CksHs1. The interaction sites in these proteins mainly consist of Arginine and Lysine, side chains binding to the decavanadate anion. To get further knowledge regarding non-covalent interactions of decavanadate in protein environments, guanidinium and spermidinium decavanadates were synthesized, crystallized, and subjected to analysis utilizing various techniques, including FTIR, Raman, ^{51}V-NMR, TGA, and X-ray diffraction. The DFT calculations were employed to calculate the interaction energy between the decavanadate anion and the organic counterions. Furthermore, the Quantum Theory of Atoms in Molecules (QTAIM) and Non-covalent Interaction-Reduced Density Gradient (NCI-RDG) analyses were conducted to understand the non-covalent interactions present in these adducts. Decavanadate can engage in electrostatic forces, van der Waals, and hydrogen bond interactions with guanidinium and spermidinium, as shown by their respective interaction energies. Both compounds were highly stabilized by strong hydrogen bond interactions N–H···O and weak non-covalent interactions C–H···O. In addition, the interactions between guanidinium and spermidinium cations and decavanadate anion form several stable rings. This

study provides new information on non-covalent intermolecular interactions between decavanadate and small biomimetic models of arginine and lysine lateral chains in protein environments.

KEYWORDS

decavanadate, guanidinium, spermidinium, biomimetic models, protein interactions, arginine and lysine side chains, non-covalent interactions

1 Introduction

The initial discovery of Vanadium occurred in a mine located in Hidalgo State, Mexico, and it is attributed to mineralogist Don Andres Manuel del Río (Caswell, 2003; Sanchéz-Lara et al., 2019; Sanchéz-Lara et al., 2020; Treviño et al., 2019). However, for historical reasons, Nils Gabriel Sefström named Vanadium according to Vanadis, which corresponds to the Scandinavian goddess of beauty and fertility (Van Cleave and Crans, 2019; Singh and Singh 2021). Since then, it has been studied, and nowadays, investigations have increased exponentially. This block-d metal has many uses and applications, to name a few, in the iron and steel industry (Barceloux and Barceloux, 1999; Moskalyk and Alfantazi, 2003), and researchers in materials science have described its potential use in the field of electrochemistry as energy storage (Rao et al., 2011; Ghosh et al., 2023). In biology and medicine, Vanadium compounds have been used to fight parasitic infections like American trypanosomiasis, malaria, and leishmaniasis (Aureliano and Ohlin, 2014; Duan et al., 2018; Del Carpio et al., 2018; Pessoa et al., 2015; Casarrubias-Tabarez et al., 2023). They have also been used as an active component of pharmaceutical drugs in treating diabetes (Tsiani and Fantus, 1997; Cuevas et al., 2012; Treviño et al., 2016). Also, in cancer therapy (Evangelou, 2002; Barrio and Etcheverry, 2010; Hartung et al., 2015; Pisano et al., 2019; Manganaro et al., 2022). In an industrialized world, factors like stress are causing people to suffer from certain types of diseases like obesity, diabetes mellitus, cancer, and neurodegenerative diseases; in this sense, Vanadium compounds are a good strategy for treating them (Contreras-Cadena et al., 2014; Treviño et al., 2016; Bijelic et al., 2018; Crans et al., 2018; Sánchez-Lara et al., 2018; Bijelic et al., 2019; Crans et al., 2019; Ferretti and León, 2022; Chen et al., 2023; Gonzalez-Cano et al., 2023).

Polyoxidometalates (POMs, formerly known as polyoxometalates) and polyoxidovanadates (POVs, formerly known as polyoxovanadates) have been the subject of extensive research in the last 30 years (Gumerova and Rompel, 2020; Pessoa et al., 2021). These chemicals have been linked to blocking enzymes (Bougie and Bisaillon, 2006; Stephan et al., 2013; Patel et al., 2019; Zhao et al., 2020) and many diseases. For example, they are used to make insulin work better in people with diabetes and stop the buildup of amyloid β-peptides that are linked to Alzheimer's disease (Treviño et al., 2016; Treviño et al., 2023; García-García et al., 2023). Polyoxidometalates (POMs) are gaining significant importance due to their properties and striking structures (Gumerova and Rompel, 2018). For example, the anion decavanadate is the most investigated because of its ability to interact with proteins (Aureliano and Gândara, 2005; Krivosudský et al., 2019; Patel et al., 2019). It is important to mention the pioneering work of Debbie Crans regarding small models for the interaction of decavanadate and proteins. The article "X-ray Structure of $(NH_4)_6(Gly\text{-}Gly)_2V_{10}O_{28}\cdot 4H_2O$: Model Studies for Polyoxometalate-Protein Interactions" started the quest to understand the role of non-covalent interactions in polyoxidometalates and proteins (Crans, 1994; Crans et al., 1994). Also, researchers have been looking into decavanadate and how it works with proteins in membrane receptors that make them act like noradrenaline (Venkataraman et al., 1997). Recently, research has focused on pharmacological uses such as antidiabetic, antibacterial, antiviral, antiprotozoal, and anticancer (Crans et al., 2004; Aureliano et al., 2022; Casarrubias-Tabarez et al., 2023; Dridi et al., 2024).

Decavanadate (V_{10}) is a simple anion compared to other POMs, but it can show how highly charged and hydrated metal oxide clusters interact with biomolecules (Aureliano and Crans, 2009). Its effects on proteins are significant. How specific V_{10}-induced structural modifications affect native proteins is crucial to understanding the mechanism of V_{10}-protein interaction. In the long term, it could help reduce V_{10}'s adverse effects on proteins in Vanadium poisoning. Proteins stabilize decavanadates in solution, mostly with arginine and lysine side chains; thus, understanding the non-covalent interactions between decavanadate and proteins is essential (Aureliano et al., 2022). Although it is already known that decavanadate is implicated in several cellular pathways, many details have yet to be discovered. For that reason, it is necessary to make an effort to study protein-decavanadate interactions in more detail. (Aureliano and Ohlin, 2014).

In this work, small biomimetic models based on guanidinium and spermidinium decavanadates were synthesized and crystallized to gain further knowledge regarding the non-covalent interactions of decavanadate in protein environments. PBE0/Def2SVP-LANL2DZ calculations were employed to determine the interaction energy between the decavanadate anion and the respective organic compounds mimicking the amino acids. We also used the Quantum Theory of Atoms in Molecules (QTAIM) and Non-covalent Interaction-Reduced Density Gradient (NCI-RDG) analyses to learn more about the non-covalent interactions in these adducts. The interaction energies of guanidinium and spermidinium ions show that decavanadate can interact with them through electrostatic forces, van der Waals forces, and hydrogen bonds. To determine the role electrostatic interactions, van der Waals forces, and hydrogen bonds play in proteins that have crystallized with the decavanadate anion, it is important to measure the non-covalent interactions in small biomimetic models. This will help us understand how decavanadate (V_{10}) behaves differently than vanadate (V_1) (Aureliano et al., 2016). Here, a contribution to this understanding is presented.

2 Materials and methods

2.1 Synthesis

2.1.1 Compound 1

All the reagents utilized were purchased from Sigma-Aldrich (Merck-Mexico). No further purification was needed, and they were

used as received. Guanidinium-Decavanadate (D10G) was synthesized in two steps. In the first one, 121 mg (1 mmol) of Sodium Metavanadate ($NaVO_3$) was dissolved in 20 mL of distilled water and stirred with a magnetic bar. After that, four drops of glacial acetic acid were added until pH = 4.5, and then 60 mg (0.57 mmol) of guanidinium hydrochloride was dissolved in 20 mL of distilled water. In the second step, both solutions were mixed, and a yellow-orange powder immediately precipitated. The mother liquor was allowed to stand at room temperature to get crystals of the compound, and as soon as the crystals were formed, they were filtered (64%).

2.1.2 Compound 2

The synthesis of Spermidinium-Decavanadate (D10SP) was as follows: using 138 mg (1 mmol of Potassium Metavanadate) (KVO_3) and 0.313 mL (0.290 mg = 0.2 mmol) of spermidine. To get decavanadate, the KVO_3 was dissolved in 20 mL of distilled water, and glacial acetic acid was added dropwise until pH = 4.2; the final solution turned bright yellow-orange. Similarly, 313 μL of spermidine were dissolved in 20 mL of distilled water. After that, the Spermidine solution was dropped slowly over the decavanadate solution. Then, a yellow-orange powder was obtained. It was filtered, and the mother liquor was allowed to stand at room temperature to obtain crystals of enough quality for X-ray diffraction. (73% yield).

2.2 Experimental characterization

The infrared spectrum was recorded using an Attenuated Total Reflectance Spectrometer (ATR) model ALPHA II Platinum Bruker, ranging from 4,000 to 400 cm^{-1} (24 scan/sample) with a resolution of 4 cm^{-1}. The RAMAN spectra were obtained with a Lab-RAM®-HORIBA JOBIN YVON, placed in the range from 500 to 1,200 cm^{-1} at room temperature. The ^{51}V-NMR spectrum was obtained using a Bruker AVANCE III 500 MHz spectrometer. Samples were prepared by dissolving ca. 5 mg/mL of the compounds in 10% D_2O solutions at pH = 5. For the X-ray diffraction, data were collected with an Oxford Diffraction Gemini-Atlas diffractometer equipped with a charge-coupled device area detector and graphite monochromated Mo-Kα radiation (λ = 0.71073 Å) (Sheldrick, 2015). Thermogravimetric analysis (TGA) with simultaneous differential thermal analysis (DTA) was carried out under an N_2 inert atmosphere on an STA 2500 Regulus (Netzsch Instruments, Selb, Germany). Samples were weighed (~10 mg) and heated from 30°C to 700°C at a heating rate of 25°C/min in alumina pans. An empty pan was used as a reference.

2.3 Software

The data were processed with the APEX3 suite, and SADABS-2016/2 was used for absorption correction (CrysAlisPro, 2013). The structure was solved by direct methods using the ShelXT program and refined by full-matrix least-squares on F^2 with SHELXL-2019 (Sheldrick, 2015). The positional and anisotropic atomic displacement parameters were refined for all non-hydrogen atoms. Hydrogen atoms were located in different Fourier maps and included as fixed contributions riding their parent atoms, with isotropic thermal factors chosen as 1.2 times their carrier atoms. The OLEX2 software (Dolomanov et al., 2009) was used as a graphical interface. Crystallographic data (excluding structure factors) for the structure reported in this paper have been deposited in the Cambridge Crystallographic Data Center. (CCDC numbers 2359514, 2359517). Mercury (Version 2022 3.0) was used to represent the crystallographic data.

2.4 Theoretical methodology

The structural and electronic structures of Compounds 1 and 2 were calculated using the density functional theory, DFT (Parr and Yang, 1989). The hybrid functional PBE0 (Adamo and Barone, 1999) was used, using the Def2-SVP basis set for the atoms of C, H, O, and N (Weigend and Ahlrichs, 2005) and the LANL2DZ basis set for the atom of V with an effective core potential (ECP) (Hay and Wadt, 1985). The PCM model used water as a solvent (Tomasi et al., 2005). The molecular structures, frontier molecular orbitals (highest occupied molecular orbital, HOMO, and lowest unoccupied molecular orbital, LUMO), and the molecular electrostatic potential (MEP) map were analyzed. The calculations were performed with the Gaussian program16 (Frisch et al., 2016), and the results were visualized with the Gaussian View 6.0.16 program (Dennington et al., 2016). Additionally, the main non-covalent interactions in Compounds 1 and 2 were characterized using the atoms in molecules (AIM) approach with AIMAll software (Keith, 2019) and Non-covalent Interaction-Reduced Density Gradient (NCI-RDG) analysis with Multiwfn software (Lu and Chen, 2012) and VMD software (Humphrey et al., 1996).

3 Results

3.1 Structural descriptions

Decavanadate cluster anion $[V_{10}O_{28}]^{6-}$ can form ionic compounds with inorganic and organic cations. It is constructed by ten edge-shared VO_6 octahedra with D_{2h} symmetry, eight terminal oxygens ($V{=}O_t$), fourteen doubly bridged oxygens (μ_2), four triply bridged oxygens (μ_3), and two hexa-bridged oxygen atoms (μ_6) (Amanchi and Das, 2018).

The crystal structure of Compound 1, $(CH_6N_3)_6$ $[V_{10}O_{28}]\cdot 6H_2O$, has been previously reported (Wang et al., 1993; Ghosh et al., 2023), and all the crystallographic parameters are essentially equal (Table 1). To summarize, the structure contains six guanidinium $(CH_6N_3)^+$ *per* $[V_{10}O_{28}]^{6-}$ anion and six lattice water molecules, which together form an extensive hydrogen bond network (Figure 1A).

On the other hand, the combination of spermidinium and decavanadate is first observed in this work, resulting in Compound 2. Thus, a more detailed description is given. Good-quality orange prism crystals of Compound 2 were obtained slowly from solvent evaporation at room temperature. This material crystallizes in the triclinic space group P 1^-, and its asymmetric unit consists of one triple protonated spermidinium $(C_7H_{19}N_3)^{+3}$, one-half of a $[V_{10}O_{28}]^{6-}$ anion located in an inversion center, and

10.3389/fchbi.2024.1451167

TABLE 1 Crystallographic data and structure refinement details.

	Compound 1 $(CH_6N_3)_6$ $[V_{10}O_{28}]\cdot 6H_2O$	Compound2 $(C_7H_{19}N_3)_2$ $[V_{10}O_{28}]\cdot 4H_2O$
Formula	$C_6H_{48}N_{18}O_{34}V_{10}$	$C_{14}H_{52}N_6O_{32}V_{10}$
CCDC	2359514	2359517
M_r ($g\cdot mol^{-1}$)	1426.02	1326.01
T (K)	293 (2)	293 (2)
Crystal system	Monoclinic	Triclinic
Space group	$P2_1/n$	P-1
a (Å)	9.22230 (10)	9.9696 (3)
b (Å)	21.9392 (2)	10.5261 (2)
c (Å)	11.1906 (2)	11.5573 (3)
a (°)	90	96.544 (2)
β (°)	103.9410 (10)	105.536 (2)
γ (°)	90	115.897 (2)
V ($Å^3$)	2197.50 (5)	1013.17 (5)
Z	2	1
r_{calc}($g\cdot cm^{-3}$)	2.155	2.173
μ (mm^{-1})	2.144	2.305
R_{int}	0.0591	0.0472
GoF on F^2	1.077	1.033
Final R indexes [I>2σ(I)]	R_1 = 0.0292, wR_2 = 0.0612	R_1 = 0.0311, wR_2 = 0.0722
Final R indexes [all data]	R_1 = 0.0502, wR_2 = 0.0701	R_1 = 0.0516, wR_2 = 0.0813

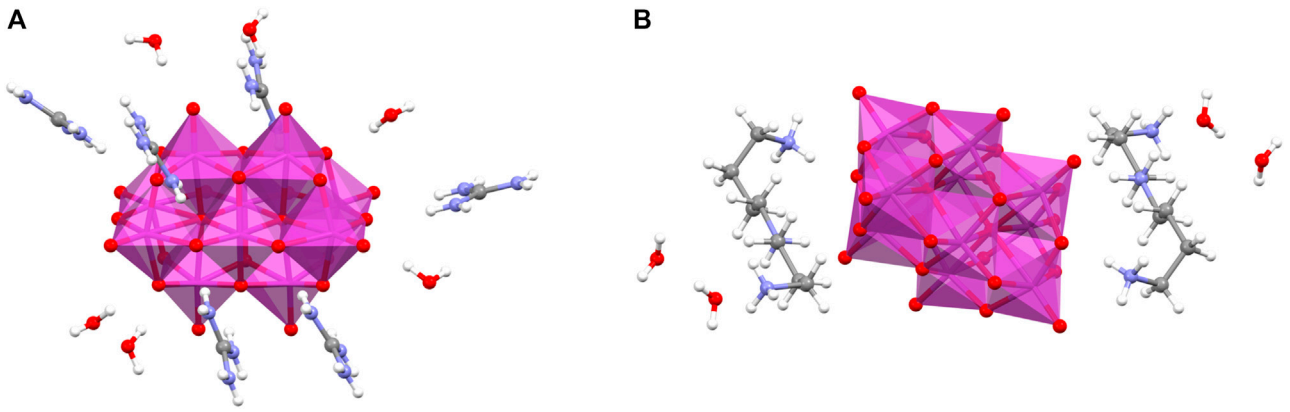

FIGURE 1
Details of **(A)** Compound 1, $(CH_6N_3)_6$ $[V_{10}O_{28}]\cdot 6H_2O$, and **(B)** Compound 2, $(C_7H_{19}N_3)_2$ $[V_{10}O_{28}]\cdot 4H_2O$. Color code: carbon, gray; nitrogen, blue; oxygen, red; Vanadium, purple; hydrogen, white.

two crystallization water molecules, giving the global formula $(C_7H_{19}N_3)_2$ $[V_{10}O_{28}]\cdot 4H_2O$. Since the decavanadate anion is completely deprotonated, two $(C_7H_{19}N_3)^{+3}$ molecules balance the six negative charges in the unit cell (Figure 1B). Table 1 compiles the experimental details of the single-crystal experiment. The checkcif for both compounds is presented in the Supplementary Material Section.

In Compound 2, the terminal V=O bond lengths fall between 1.599 (1) and 1.624 (1) Å. In the case of μ_2–O atoms, the V–O bond distances increase and vary from 1.690 (1) to 2.078 (1), whereas the V–O bond

10.3389/fchbi.2024.1451167

TABLE 2 Distances (Å) and angles (°) of the main hydrogen bonds of Compound 1 and 2.

Compound 1				
D-H···A	d (D-H)/Å	d (H···A)/Å	d (D···A)/Å	D-H···A/°
N1-HA1···O8	0.86	2.12	2.9457 (19)	161.3
N3-H3A···O20	0.86	2.04	2.9007 (19)	179.6
N4-H4B···O16	0.86	2.18	2.9419 (19)	147.7
N7-H7B···O22$^{(i)}$	0.86	2.17	2.887 (3)	140.6
N8-H8B···O23$^{(ii)}$	0.86	2.16	2.919 (3)	146.4
N9-H9A···O15$^{(i)}$	0.86	2.11	2.8491 (19)	143.7
N9-H9B···O23$^{(ii)}$	0.86	2.08	2.857 (2)	149.4
O22-H22A···O24$^{(iii)}$	0.85	1.91	2.750 (2)	171.6
O22-H22B···O9	0.85	2.10	2.9378 (19)	170.4
O23-H23A···O9	0.85	1.93	2.7614 (18)	164.9
O23-H23B···O10$^{(iv)}$	0.85	2.04	2.8731 (19)	168.7
O24-H24A···O13$^{(i)}$	0.93	2.00	2.8812 (19)	159.3
O24-H24B···O17	0.85	2.06	2.887 (7)	162.8
Compound 2				
D-H···A	d(D-H)/Å	d(H···A)/Å	d(D···A)/Å	D-H···A/°
N1-H1A···O13	0.89	1.87	2.7431 (18)	167.7
N1-H1B···O18$^{(v)}$	0.89	2.10	2.8732 (18)	144.6
N2-H2A···O20	0.89	1.90	2.7732 (19)	164.9
N2-H2B···O21	0.89	1.97	2.770 (2)	148.9
N3-H3A···O9$^{(vi)}$	0.89	1.94	2.7658 (18)	153.5
N3-H3B···O16$^{(vii)}$	0.89	1.99	2.8078 (19)	151.5
N3-H3C···O14$^{(viii)}$	0.89	2.01	2.8921 (19)	170.1
O21- H21A···O22	0.85	1.90	2.740 (2)	171.9
O22-H22A···O7$^{(viii)}$	0.85	1.89	2.7358 (17)	170.3
O22-H22B···O7$^{(ix)}$	0.85	2.10	2.9363 (19)	168.5

Symmetry codes: (i) −½+x, ½-y, −½+z; (ii) ½+x, ½-y, −½+z; (iii) x, y, 1+z; (iv) 1-x, 1-y, 2-z; (v) −1+x, −1+y, z; (vi) 2-x, 2-y, 1-z; (vii) 1-x, 2-y, 1-z; (viii) 1-x, 1-y, 1-z; (ix) −1+x, y, −1+z

distances for μ_3–O atoms are in the interval of 1.899 (1) to 2.035 (1) Å. Lastly, the hexacoordinated oxygen atom's V–O bond lengths range from 2.111 (1) to 2.339 (1) Å. All distances are in normal ranges, consistent with other polyoxovanadate-based structures (Evans Jr, 1966; Correia et al., 2004; Bosnjakovic-Pavlovic et al., 2011).

In both complexes, the organic linkers and the lattice water molecules create an intricate network of hydrogen bonds with the decavanadate anions that stabilize the three-dimensional solid state. Table 2 lists the most important non-covalent interactions.

Compound 1 has three symmetrically independent guanidinium cations $(CH_6N_3)^+$ containing three -NH_2 groups, which can form six hydrogen interactions with water molecules and decavanadate anions (Figure 2). Some of these non-covalent interactions are not shown in Table 2 because their D···A distances are larger than 3.0 Å.

Within the structure, the guanidinium cations and lattice water molecules encircle the $[V_{10}O_{28}]^{-6}$ clusters, creating an extensive hydrogen bond network (Figure 3A). However, interestingly, if all organic cations were eliminated, the water molecules would retain the robust three-dimensional structure with decavanadate anions (Figure 3B).

Similarly, the supramolecular structure of Compound 2 is dominated by N-H···O and O-H···O interactions involving all spermidinium, water molecules, and decavanadate anions. In this structure, spermidinium cations are triply protonated at N1, N2, and N3 atoms, resulting in a (+3)-positive charge and eight available donor H atoms present for hydrogen bonding (Figure 4).

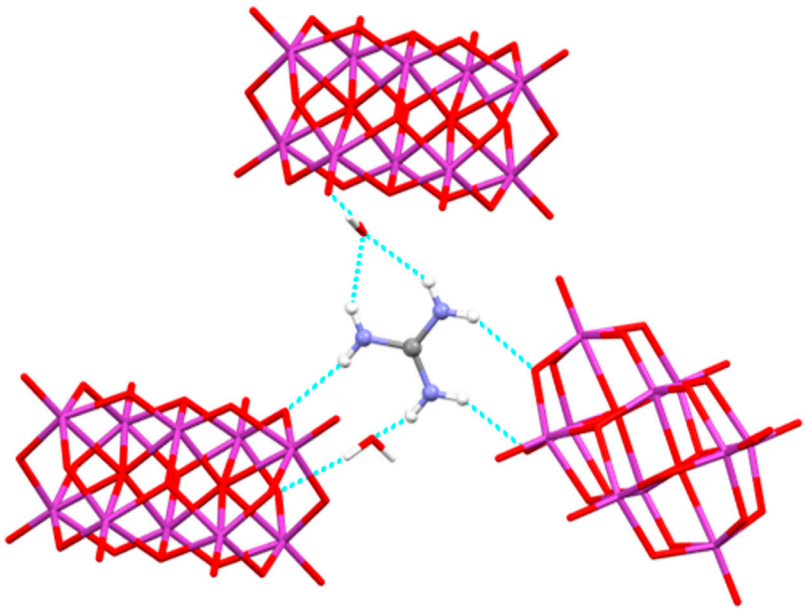

FIGURE 2
A single guanidinium molecule surrounded by three decavanadate anions in Compound 1.

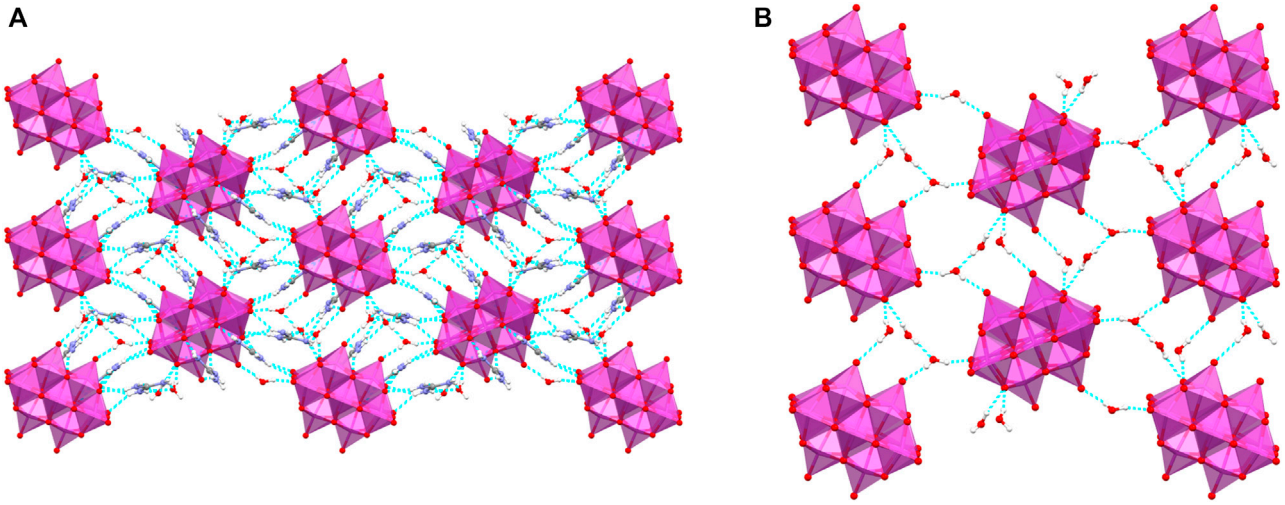

FIGURE 3
(A) Supramolecular structure of Compound 1 along *a* crystallographic axis; **(B)** if guanidinium molecules were removed, lattice water molecules would retain the 3D structure. Hydrogen bonds are drawn as dotted light blue lines.

The resulting crystal structures are densely packed systems in which hydrogen bonds are crucial for holding both compounds. Theoretical studies have been carried out to analyze these non-covalent interactions.

3.2 Infrared spectroscopy

The anion decavanadate is a rigid cluster of atoms with only a few principal vibrations; however, it is nontrivial to assign them, even more so if the vibrational modes are coupled with those of the amino acids. The experimental and theoretical spectra of Compounds 1 and 2 (Figure 5) are presented in the region 1,200–400 cm^{-1}. The complete spectra of the two compounds are presented in the Supplementary Material (Supplementary Figure S1). The IR spectra of ammonium and potassium decavanadates (Supplementary Figure S2) are also presented in the Supplementary Material Section as a reference for band assignments (Supplementary Table S1). Bands resulting from the stretching vibrations of terminal $V{=}O_t$ commonly occur between 1,000 and

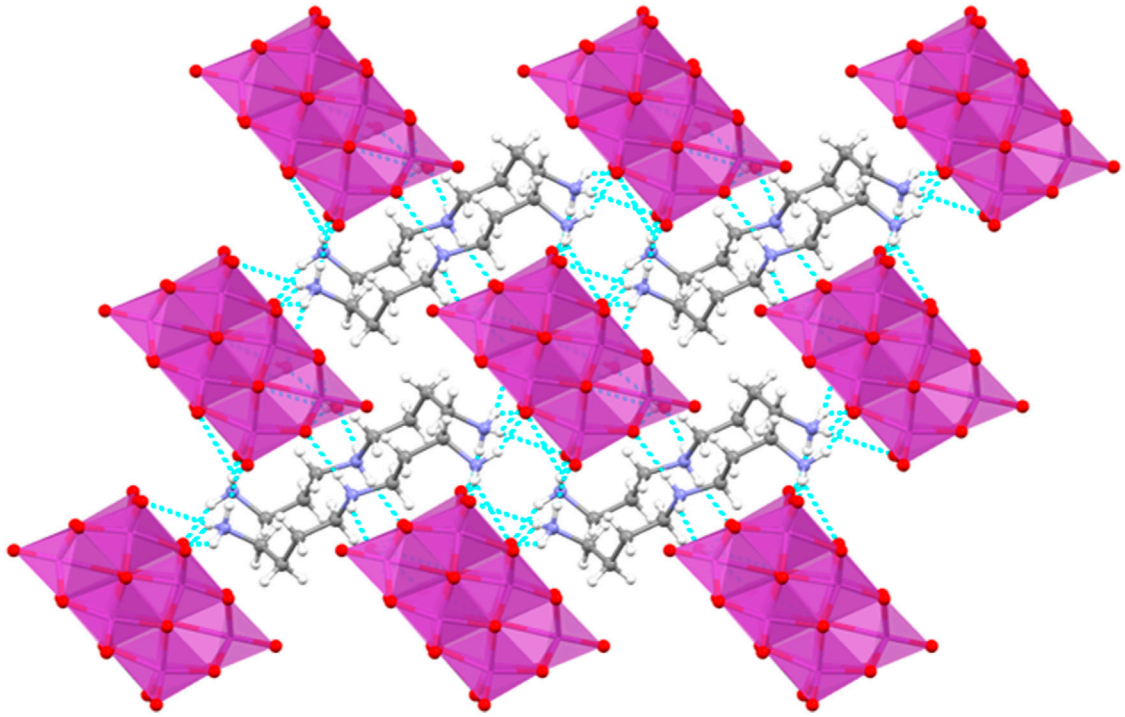

FIGURE 4
Non-covalent interactions dominate the supramolecular structure of Compound 2. Hydrogen bonds are drawn as dotted light blue lines.

910 cm^{-1}, while ν_{as} (V-O_b-V) occurs between 820 and 700 cm^{-1}. On the other hand, bands below 700 cm^{-1} could be assigned to the symmetric vibrations of the bridging (V–O_b–V). For Compound 1 (guanidinium-decavanadate, D10G), the bands at 981 and 948 cm^{-1} are caused by the terminal V=O_t bonds; the bands at 828, 804, and 734 cm^{-1} are caused by the (V-O_b-V) antisymmetric vibrations; and the bands 586, 536, and 514 cm^{-1} correspond to the symmetric vibrations (V-O_b-V). Finally, the band at 460 cm^{-1} is assigned to out-of-plane deformation. The splitting of the bands indicates different environments related to hydrogen bonds of different strengths.

In the spectrum of Compound 2 (spermidinium-decavanadate, D10SP), the band at 944 cm^{-1} corresponds to the stretching V=O_t, while the bands at 808 cm^{-1} and 726 cm^{-1} are due to the bridging antisymmetric vibration of (V-O_b-V). Finally, the bands at 582, 542, and 514 are assigned to the (V-O_b-V) symmetric vibrations. The band at 445 cm^{-1} is assigned to out-of-plane deformation. Additionally, shoulders flank the strongest peak (Rakovský et al., 2002; Biçer et al., 2017; Avila et al., 2019).

The theoretical IR spectra were performed to complement the assignment of the main vibrational modes. Leters a-g were used to distinguish the different types of oxygen atoms, according to Bartošová et al., 2012. For Compound 1, in the region of 970–921 cm^{-1} three main bands corresponding to the pure asymmetric stretching ν_{as} (V=O_t) at 952 cm^{-1}, and two coupled modes of ν_{as} (V=O_t) with asymmetric stretching ν_{as} (C=N) and in-plane bending δ(C=N–H) of guanidinium at 970 and cm^{-1} were found, respectively. At the region of 827–664 cm^{-1}, several coupled modes with ν_{as} (V=O_t) are observed, mainly in-plane bending δ(V–O_b–V), wagging ω(C=N–H), and ω(N=C–N), and out-plane bending γ(N=C–N) of guanidinium. At the 588–451 cm^{-1} coupled in-plane bending modes, δ(V–O_a–V), δ(V–O_c–V), and δ(V–O_e–V) are observed, involving several types of oxygen atoms, contributing to internal deformations of decavanadate anion. In addition, in-plane bending modes δ(C=N–H) of guanidinium are observed. For Compound 2, in the region of 960–909 cm^{-1}, it is assigned to ν_{as} (V=O_t) coupled with δ(C–C–H) and δ(C–N–H) of spermidinium. At the region at 812–787 cm^{-1}, coupled δ(V–O_b–V) with ν_{as} (V–O_e) and ν_{as} (C–N) of spermidinium are observed. Several bands at 722–508 cm^{-1} are assigned to different in-plane bending involving different types of oxygen atoms, as δ(V–O_a–V), δ(V–O_b–V), δ(V–O_c–V) and δ(V–O_e–V). Finally, in the region, 482–447 cm^{-1} in-plane bending internal deformations of decavanadate are coupled with the rocking mode of spermidinium ρ(N–H_3). These findings align with previous experimental and theoretical FT-IR spectra reported for similar compounds (Guilherme et al., 2010; Sánchez-Lombardo et al., 2014; Sánchez-Lara et al., 2015; Sánchez-Lara et al., 2018; Sánchez-Lara et al., 2019; García-García et al., 2021; Corona-Motolinia et al., 2022). Shifts of the main bands with respect to the ammonium decavanadate are presented in Supplementary Table S2. It is seen that the strong hydrogen bonds in the guanidinium decavanadate mainly impact the V=O_t stretching frequencies, although there are slight shifts in the other bands. The behavior of the spermidinium decavanadate is very similar to the ammonium decavanadate.

3.3 Raman spectroscopy

The experimental and theoretical spectra of Compounds 1-2 (Figure 6) are presented in the region 1,150–500 cm^{-1}. The

10.3389/fchbi.2024.1451167

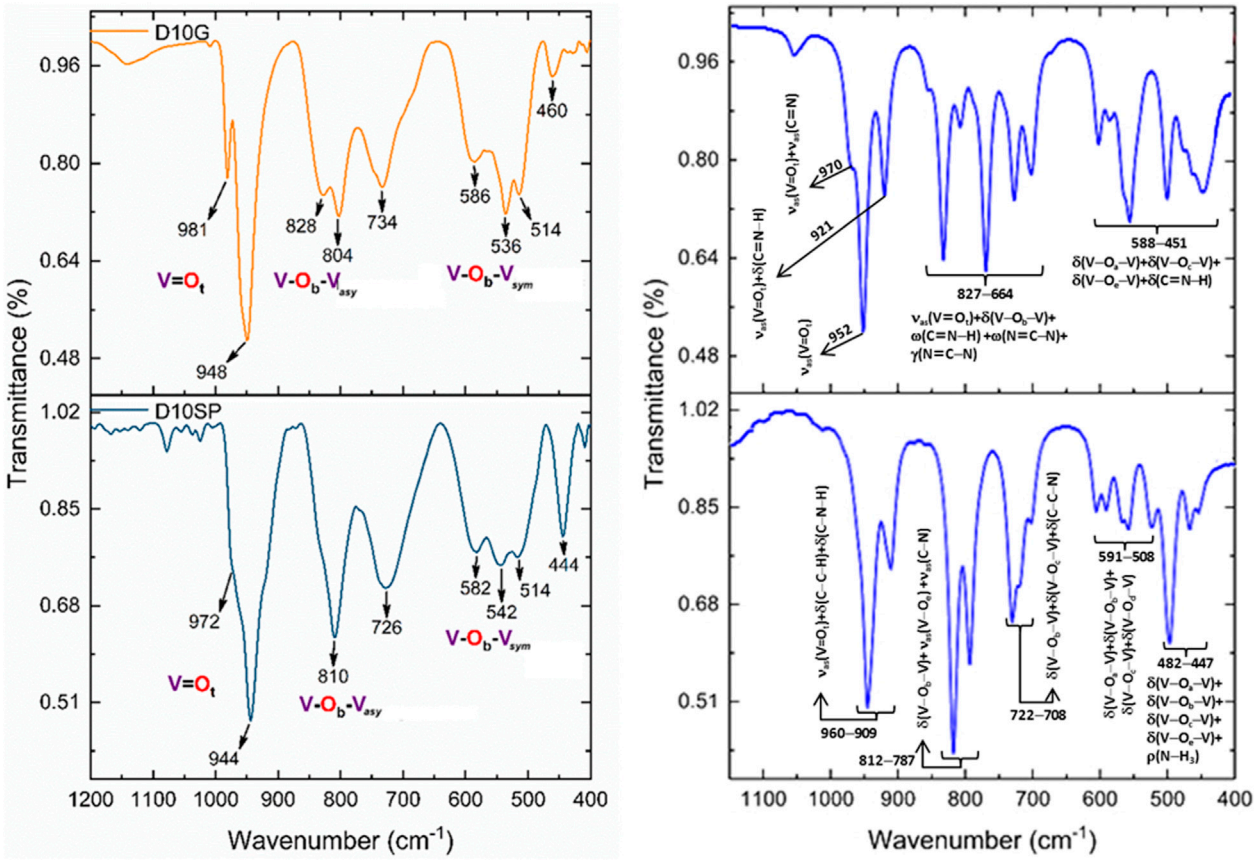

FIGURE 5
Experimental (left) and theoretical (right) FT-IR spectra of Compounds 1 and 2 in the region of VO vibrations.

complete spectra are presented in the Supplementary Material section (Supplementary Figure S3). The experimental Raman spectrum for Compound 1 has three prominent peaks at 1,016, 996, and 969 cm^{-1}, which correspond to V=O_t stretching, and one more in the region of 832 cm^{-1}, which corresponds to an antisymmetric vibration. For Compound 2, the Raman spectrum also shows three prominent peaks at 989, 966, and 928 cm^{-1}, which can be assigned to the stretching vibration V=O_t, and one more at 835 cm^{-1}, which is a coupled mode of in-plane bending vibrations. A complete list of assignments is presented in Supplementary Table S3. Due to the significant symmetry of the decavanadate anion, a simple spectrum is expected. However, due to the hydrogen bond interactions of different magnitudes, it is challenging to simplify the assignment of each vibrational mode. Nevertheless, modes with high frequencies (900 cm^{-1} and above) are predominantly characterized by V=O_t stretching. The ν_{asym} (O–V_b–O) movement exhibits significant intensity at slightly lower frequencies. (Todorović et al., 2005; Frost and Palmer, 2011; Omri et al., 2015; Aureliano, 2016; Sánchez-Lara et al., 2016; Baran, 2024). Shifts of the main bands with respect to the ammonium decavanadate are presented in Supplementary Table S3. The shifts are less pronounced in the Raman spectra than in the IR spectra. However, the V=O_t signals are better defined than in the IR spectra.

The theoretical Raman spectrum of Compound 1 shows coupled modes of ν_s (V=O_t) with stretching ν_s (C–N) at 1,011 cm^{-1} and with in-plane bending δ(H–N–H) and δ(C–N–H) of guanidinium, at 995 cm^{-1} and 959 cm^{-1}, respectively. The band at 819 cm^{-1} is assigned to coupled modes of in-plane bending of δ(V–O_c–V) and δ(V–O_d–V) of decavanadate with wagging ω(C–N–H) of guanidinium. At the regions of 612–563 cm^{-1} and 544–519 cm^{-1} are observed several in-plane bending involving the different types of oxygen atoms in decavanadate δ(V–O_a–V), δ(V–O_b–V), δ(V–O_c–V), and δ(V–O_d–V), coupled with rocking ρ(N–H_2) or in-plane bending δ(N–C–N) of guanidinium. For Compound 2, the spectrum shows the pure symmetric stretching ν_s (V=O_t) at 984 cm^{-1}, and two coupled modes of ν_s (V=O_t) with symmetric stretching ν_s (C–C) and ν_s (C–N), and in-plane bending δ(C–C–N) of spermidinium, at 960 and 946 cm^{-1}, respectively. The bands in the region of 846–828 cm^{-1} are assigned to coupled modes of ν_s (V–O_e) with several in-plane bending δ(V–O_c–V), δ(V–O_d–V), and δ(V–O_e–V) of decavanadate. Finally, at the region of 611–540 cm^{-1} are observed several in-plane bending δ(V–O_a–V), δ(V–O_b–V), δ(V–O_c–V), and δ(V–O_e–V), coupled with the symmetric torsion τ(SP) of spermidinium as a whole.

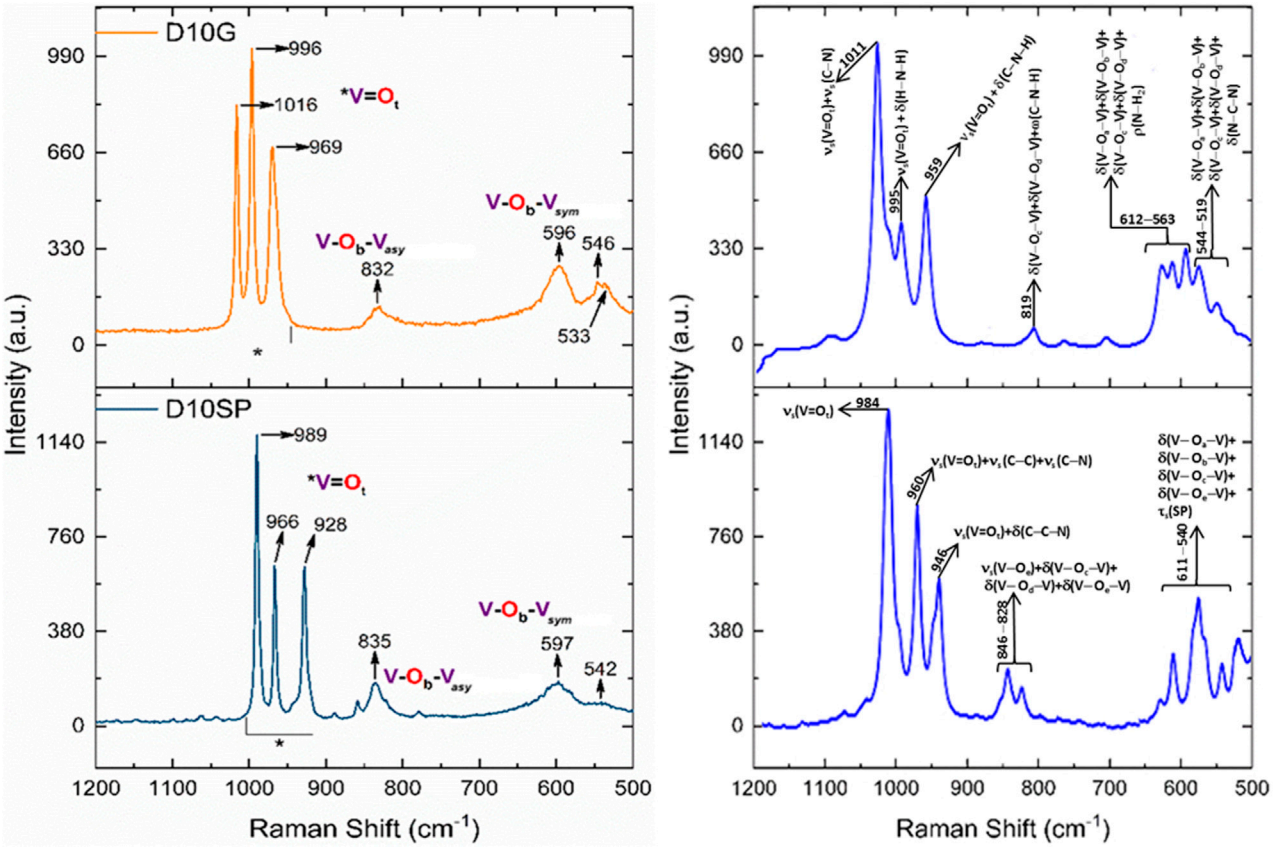

FIGURE 6
Experimental (left) and theoretical (right) Raman spectra of Compounds 1 and 2 in the region of VO vibrations.

3.4 ^{51}V nuclear magnetic resonance

Figure 7 presents the ^{51}V NMR spectrum of Compound 1 obtained at room temperature at a pH near 5. Three principal peaks at δ −422.04, δ −497.71, and δ −513.22 ppm due to the different types of V atoms. The peak at δ −422 corresponds to V10C, the peak at δ −497.71 to V10B, and V10A occurs at δ −513.22. The other peaks are due to the decomposition of the anion decavanadate into vanadate V_1, divanadate V_2, and tetravanadate ions V_4. (Rehder, 2008; Rehder, 2015a; Omri et al., 2015). The weight of Compound 1, used to perform the experiment, was 5 mg, diluted in 1 mL of D_2O. The resonance tube was filled with 500 μL of this dissolution.

Figure 8 presents the ^{51}V NMR spectrum of Compound 2 at a pH near 5, taken immediately after the compound's synthesis. As described previously in Figure 7, the spectrum has three principal peaks. The peak observed at δ −558 ppm, labeled as V1, is associated with the decomposition of the decavanadate into its monomer. For Compound 2, the experiment was performed similarly to Compound 1, which used 5 mg and 500 μL of dissolution. In Table 3, a comparison of ^{51}V NMR bands with the ones obtained for potassium decavanadate is presented.

The spectrum of potassium decavanadate was determined under the same conditions to serve as a control for small shifts in the vanadium bands.

3.5 TGA and DTA studies

The thermal behavior of $(CH_6N_3)_6$ $[V_{10}O_{28}]\cdot 6H_2O$ (Compound 1) and $(C_7H_{19}N_3)_2$ $[V_{10}O_{28}]\cdot 4H_2O$ (Compound 2) were determined by TGA/DTA analysis (Figures 9, 10). For Compound 1 (Figure 9), the thermogram shows an exothermic mass loss of around 7.5%. This corresponds with the loss of six water molecules from the crystal lattice from 50°C to 100°C [% mass, calc. (found): 7.6% (7.5%)]. The following thermal event happens around 241°C, close to guanidinium's melting point. An endothermic process follows this in the range of 250°C–300°C, which may be caused by the thermal breakdown of six guanidinium cation units (mass loss of about 26.5%; calculated to be 25.3%). These results agree with previous reports for similar systems (Wery et al., 1996; Siva et al., 2017). The last thermal events detected occurred in the 345°C–455°C range, which is attributed to the decomposition of the decavanadate cluster into V_2O_5.

For Compound 2 (Figure 10), the thermogram shows an exothermic event with a mass loss of about 10.5% before 100°C. This is because solvent molecules that were stuck in the crystal lattice evaporate. After this, two consecutive thermal events occur between 150°C and 350°C. This can be related to the step-by-step exothermic elimination of the two spermidinium cations, with a total mass loss of 17%. Above 350°C, the exothermic thermal decomposition of the decavanadate cluster into V_2O_5 occurred.

10.3389/fchbi.2024.1451167

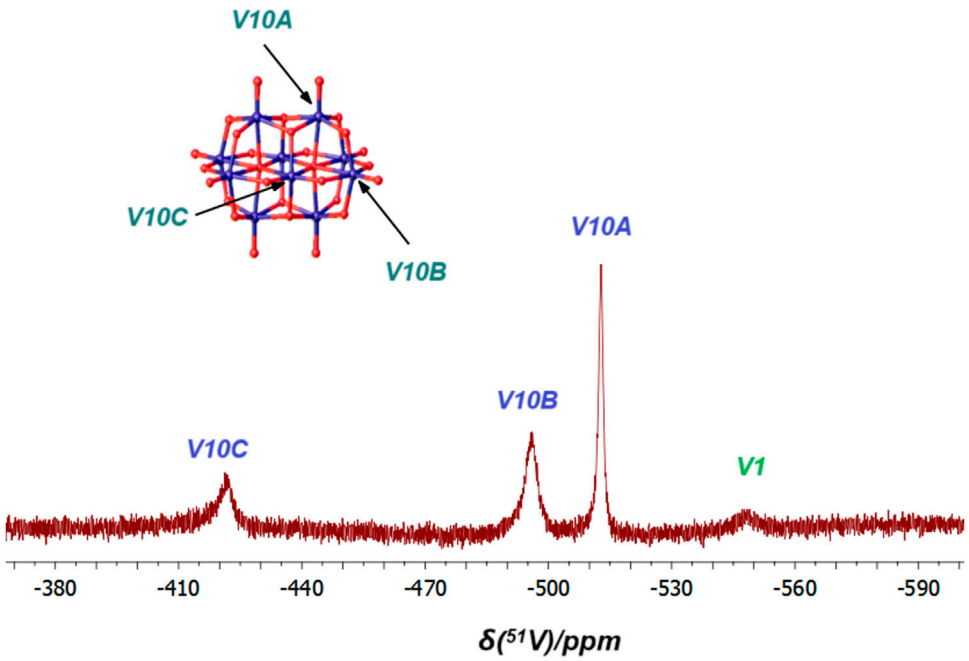

FIGURE 7
^{51}V NMR spectra of decavandate anion of Compound 1. Crystals were dissolved in 10% D_2O at pH=5.

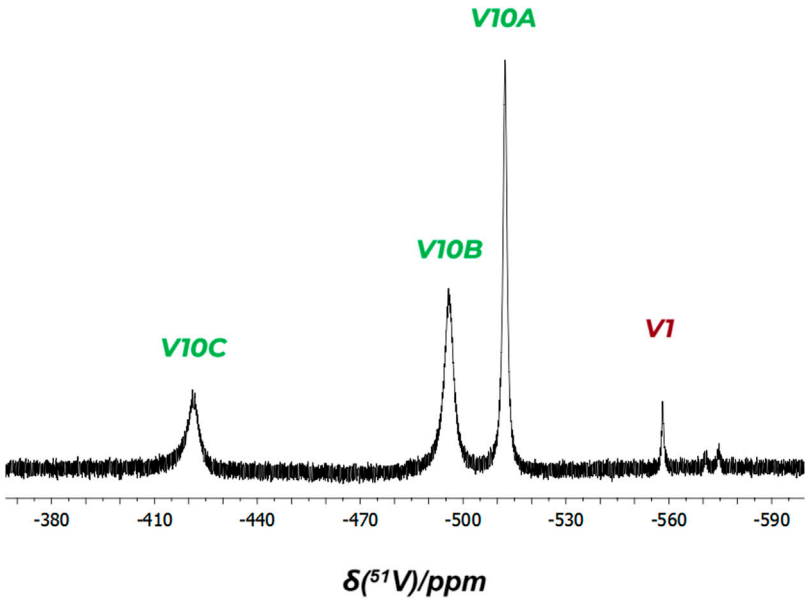

FIGURE 8
^{51}V NMR Spectra of decavanadate anion of Compound 2. Crystals were dissolved in 10% D_2O at pH=5.

TABLE 3 ^{51}V **NMR Values of potassium decavanadate, Compound 1 and Compound 2.**

51V	Potassium decavanadate	Guanidinium decavanadate	Spermidinium decavanadate
Vc, Vb, Va	424, 501, 515	422, 500, 515	425, 504, 521

It is seen that the ^{51}V signals are equal within the experimental error.

10.3389/fchbi.2024.1451167

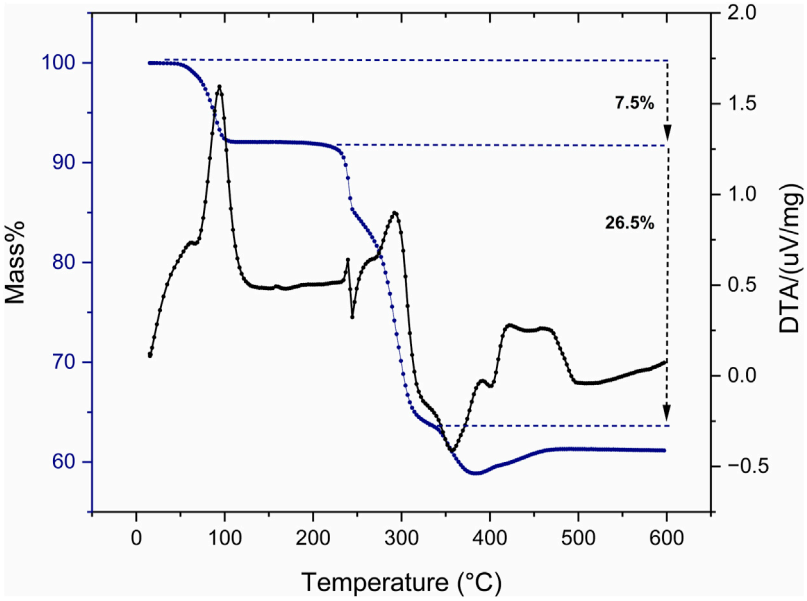

FIGURE 9
TGA/DTA of Compound 1 $(CH_6N_3)_6$ $[V_{10}O_{28}]$●$6H_2O$.

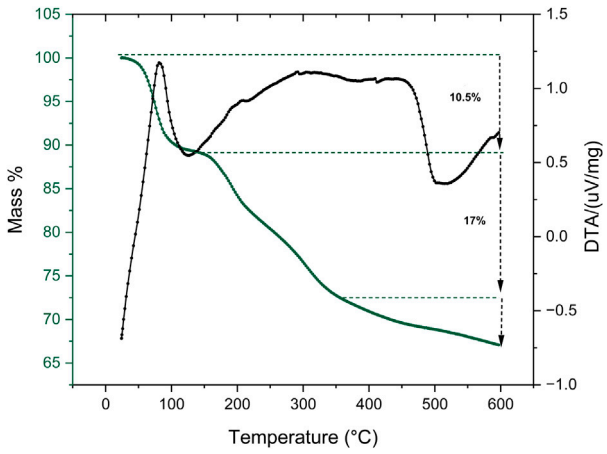

FIGURE 10
TGA/DTA of Compound 2 $(C_7H_{19}N_3)_2$ $[V_{10}O_{28}]$●$4H_2O$.

3.6 Theoretical description

Table 4 shows the interaction energies, E_{int}, obtained for two fragments using the equation $E_{int} = E_{opt-complex} - (E_{frag1} + E_{frag2})$, where $E_{opt-complex}$ is the optimized energy of Compounds 1 and 2 calculated at the level of theory PBE0/Def2SVP-LANL2DZ using ECP = LANL2DZ for the V atom, E_{frag1} is the energy obtained in a single-point calculation of the decavanadate anion at the same level of theory and E_{frag2} is the energy obtained also in a single-point calculation of the fragment formed by six guanidinium and two spermidinium cations at the same level of theory for Compounds 1 and 2, respectively. It is observed that Compound 1 has the best interaction energy by 23 kcal/mol. It could be because, in Compound 1, the decavanadate anion is surrounded by more cations through twelve strong hydrogen bonds, while only four strong hydrogen bonds are found in Compound 2. Non-covalent interactions of type N–H···O and van der Waals interactions stabilize the structures, as can be explained by the QTAIM and NCI-RDG analyses.

Figure 11A shows the optimized geometry of Compound 1, whose decavanadate anion $[V_{10}O_{28}]^{6-}$ was surrounded by six guanidinium cations to obtain a neutral and singlet multiplicity model. Supplementary Figure S5 shows the isosurfaces of frontier molecular orbitals, HOMO and LUMO, and the molecular electrostatic potential (MEP) map, plotted with an isovalue of 2×10^{-2} and 4×10^{-4} a.u., respectively. Both HOMO and LUMO are mainly located on decavanadate anion, HOMO on oxygen atoms, indicating their electron donor behavior, and LUMO on vanadium atoms, indicating their electron acceptor behavior, to form non-covalent interactions with the guanidinium cations. The MEP, mapped in the range of -1.5×10^{-1} to 1.5×10^{-1}, indicates high electronic density concentrated on decavanadate anion (red regions). In contrast, the zones with electronic density depletion are located on the guanidinium cations (blue areas). The non-covalent interactions between the O atoms of decavanadate anion and H atoms of guanidinium molecules are located in intermediate electronic density zones (yellow regions), as shown in Supplementary Figure S3.

Figure 11B shows the molecular graph of Compound 1. Green dots represent bond critical points (BCP), blue dots represent ring critical points (RCP), and orange dots represent cage critical points (CCP). Figure 11B labels the main BCP as CP1-CP6, indicating strong hydrogen bonds between O atoms of decavanadate anion and H atoms linked to donor N atoms of guanidinium cations, N–H. The topological electron density parameters, ρ(r), the Laplacian of density, $\nabla^2\rho(r)$, the energy of interaction, $E_{H\cdots Y}$, the potential energy, V(r), the interatomic distance, D_{int}, and the interatomic angle, A_{int}, are shown in Table 5. Critical points CP1-CP6 show ρ(r) values from 0.0352 to 0.0518 a.u. All $\nabla^2\rho(r)$ values are positive, indicating that the non-

TABLE 4 Interaction energies, E_{int} (in kcal mol^{-1}), calculated at the level of theory PBE0/Def2SVP-LANL2DZ using ECP=LANL2DZ for the V atom.

	$E_{opt-complex}$ (u.a.)	E_{frag1} (u.a.)	E_{frag2} (u.a.)	E_{int} (u.a.)	E_{int} (kcal/mol)
Compound 1	−4051.8913	−2818.8697	−1232.7964	−0.2211	−138.77
Compound 2	−3704.7757	−2818.8697	−885.7218	−0.1842	−115.58

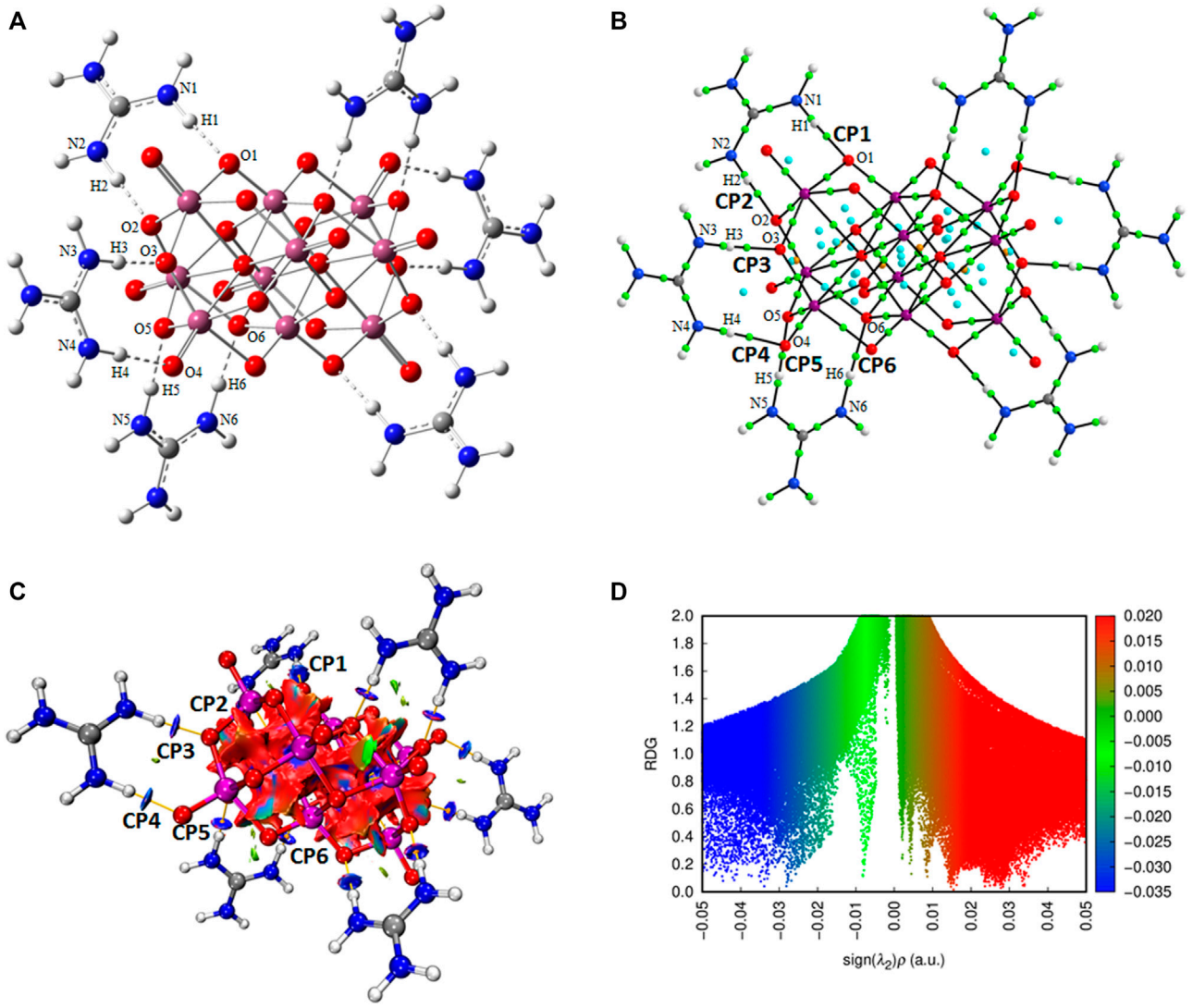

FIGURE 11
(A) Optimized structure of Compound 1 formed by one anion of $[V_{10}O_{28}]^{6-}$ linked by six guanidinium cations; **(B)** Molecular graph showing the main H bonds between the decavanadate anion and guanidinium cations; **(C)** Non-covalent Interaction (NCI) graph; and **(D)** Reduced Density Gradient (RDG) graph.

covalent interactions are hydrogen bonds. The values of interaction energy for the BCPs, obtained from V(r) values with the equation $E_{H...Y} = \frac{1}{2}|V(r)|$, are in the range of 7.81–13.68 kcal/mol, with the highest values for CP2 and CP6, indicating the most strong N–H···O hydrogen bond interactions (see Table 5). Stable rings are formed by the interactions between guanidinium cations and decavanadate anion with RCPs with ρ(r) of 0.0040–0.0045 a.u. (see Figure 11B).

Figures 11C, D show the Non-covalent Interactions (NCI) and the Reduced Density Gradient (RDG) graphs, respectively. The N–H···O hydrogen bonds between N–H of the guanidinium cations with the O atoms of the decavanadate anion are shown in blue regions labeled as CP1-CP6, observed at the range −0.05 to −0.03 a.u. In addition, some van der Waals interactions are observed as small green surfaces, mainly within the rings formed by the interactions between guanidinium and decavanadate ions, in the range of −0.02 to 0.01 a.u. Finally, strong repulsive interactions are observed in red regions of 0.015–0.05 a.u., corresponding to the atoms in the decavanadate anion.

TABLE 5 Topological parameters (in a.u.), interaction energies of BCPs, $E_{H\cdots Y}$ (in kcal mol^{-1}), interatomic distances, D_{int} (in Å), and interatomic angles, A_{int} (in degrees).

Compound 1							
	BCP	ρ(r)	$\nabla^2\rho(r)$	V(r)	D_{int}	A_{int}	$E_{H\cdots Y}$
CP1	N1-H1 . . . O1	0.0379	0.1230	−0.0280	1.769	177.37	8.79
CP2	N2-H2 . . . O2	0.0478	0.1479	−0.0387	1.680	177.48	12.14
CP3	N3-H3 . . . O3	0.0453	0.1440	−0.0359	1.698	176.74	11.26
CP4	N4-H4 . . . O4	0.0352	0.1157	−0.0249	1.791	178.49	7.81
CP5	N5-H5 . . . O5	0.0450	0.1410	−0.0354	1.704	177.52	11.11
CP6	N6-H6 . . . O6	0.0518	0.1535	−0.0436	1.653	177.89	13.68
Compound 2							
	BCP	ρ(r)	$\nabla^2\rho(r)$	V(r)	D_{int}	A_{int}	$E_{H\cdots Y}$
CP1	N1-H1 . . . O1	0.0281	0.0849	−0.0202	1.936	137.07	6.34
CP2	N1-H2 . . . O2	0.0656	0.1633	−0.0609	1.567	159.25	19.11
CP3	C3-H3 . . . O3	0.0118	0.0319	−0.0082	2.407	152.16	2.57
CP4	N4-H4 . . . O4	0.0726	0.1836	−0.0743	1.530	173.20	23.31
CP5	C5-H5 . . . O5	0.0112	0.0351	−0.0079	2.425	127.87	2.48
CP6	C6-H6 . . . O4	0.0087	0.0314	−0.0061	2.581	128.79	1.91
CP7	C7-H7 . . . O5	0.0052	0.0198	−0.0033	2.771	125.72	1.04

Figure 12A shows the optimized geometry of Compound 2. In this case, the decavanadate $[V_{10}O_{28}]^{6-}$ was surrounded by two spermidinium cations to obtain a neutral and singlet multiplicity model. Supplementary Figure S5 shows the isosurfaces of HOMO and LUMO orbitals and the MEP map, plotted with an isovalue of 2×10^{-2} and 4×10^{-4} a.u., respectively. Both HOMO and LUMO are also mainly located on the decavanadate anion. HOMO is located on the oxygen atoms of decavanadate, indicating its electron donor behavior to form non-covalent interactions with the spermidinium cations. LUMO is situated mainly on vanadium atoms, indicating its electron acceptor behavior. The MEP, mapped in the range of -1.5×10^{-1} to 1.5×10^{-1}, indicates a high electronic density concentrated on the decavanadate anion (red regions). The zones with electronic density depletion are located on the spermidinium cations (blue areas), especially in the ammonium terminal group. The non-covalent interactions between the O atoms of the decavanadate anion and the H atoms of spermidinium molecules are located in intermediate electronic density zones (yellow regions), as shown in Supplementary Figure S5.

Figure 12B shows the molecular graph of Compound 2. The main BCPs are labeled as CP1-CP7. The topological electron density parameters shown in Table 5 indicate that critical points CP1, CP2, and CP4, with values of ρ(r) at the range of 0.0281–0.0726 a.u., correspond to hydrogen bonds between O atoms of decavanadate anion with H atoms linked to donor N atoms of spermidinium cations, $^{+}$N–H. The highest positive values of $\nabla^2\rho(r)$ indicate that the non-covalent interactions are hydrogen bonds: 0.0849, 0.1633, and 0.1836 u.a. for CP1, CP2, and CP4, respectively. Critical points CP2, CP5-CP7 with values of ρ(r) of 0.0052–0.0118 a.u. and of $\nabla^2\rho(r)$ of 0.0198–0.0351 a.u. are weak non-covalent interactions C-H···O. The values of interaction energy of BCPs for strong hydrogen bonds are 19.11 and 23.31 kcal/mol for CP2 and CP4, respectively (see Table 5). Stable rings are formed by the interactions between spermidinium cations and decavanadate anion with RCPs with ρ(r) of 0.0041–0.0112 a.u. (see Figure 12B).

Figures 12C, D show the NCI and RDG graphs. The N–H···O hydrogen bonds between $^{+}$N–H of the spermidinium cations with the O atoms of the decavanadate anion are shown in CP1 in a blue region. In contrast, for CP2 and CP4, these hydrogen bonds are represented by surfaces blue-red, indicating the formation of hydrogen bonds with a repulsive contribution due to the smaller D_{int} in these critical points (see Table 5). These hydrogen bonds are observed at −0.05 to −0.025 a.u. in the RDG graph. Several green surfaces are observed around critical points CP2 and CP5-CP7, indicating van der Waals interactions related to the weak non-covalent interactions C–H···O. These van der Waals interactions are observed from −0.02 to 0.005 a.u. of the RDG graph. Strong repulsive interactions are observed in red regions in the range of 0.015–0.05 a.u., corresponding to the atoms in the decavanadate anion.

4 Discussion

Research on polyoxidometalates (POMs, formerly known as polyoxometalates) has grown exponentially in the last 30 years. In particular, polyoxidovanadates (POVs) (Pope and Müller, 1991; Aureliano et al., 2021). This has extended to various basic and applied fields. Numerous studies have been published on different aspects and applications of POVs, including industrial chemistry, catalysis, environmental chemistry, materials science, biochemistry, biology, pharmacology, and medicine (Mizuno and Kamata, 2011; Rehder, 2017; Missina et al., 2018; Bijelic et al., 2019; Missina et al., 2020; Aureliano et al., 2021; Diaz et al., 2021; Aureliano et al., 2022; Aureliano et al., 2023; Budych et al., 2023; Carvalho and Aureliano, 2023; Díaz et al., 2023; Rehder, 2023; Aureliano et al., 2024; Ścibior et al., 2024). A report in 1973 that introduced V_{10} as a micromolecular inhibitor of rabbit muscle adenylate kinase (DeMaster and Mitchell, 1973) is a landmark that started an exponential trend in the research of vanadium compounds in biological systems (Rehder, 2013a; Rehder, 2013b; Rehder, 2015b). Among the most studied polioxidovanadates is decavanadate, which is a charge-6 anion that has been found in 6 proteins of great biological relevance (acid phosphatase, tyrosine kinase, two ecto-nucleoside triphosphate diphosphohydrolases (NTPDases), the human transient receptor potential cation channel (TRPM4), and the human cell cycle protein CksHs1 (Aureliano et al., 2022). Interactions with positively charged amino acids such as lysine and arginine and hydrogen-binding formers such as histidine and serine are represented in the binding sites of such proteins. However, arginine and lysine comprise the majority of side chains that interact with decavanadate (Aureliano et al., 2022). Due to the large size of the proteins, studying non-covalent interactions with the decavanadate anion is a significant challenge. To learn more about their non-covalent interactions, guanidinium and spermidinium, two small decavanadates with organic cations, were made, crystallized, and studied experimentally and theoretically in this work.

Hydrogen bonds and electrostatic interactions involving the arginine side chains of proteins are very important in biological

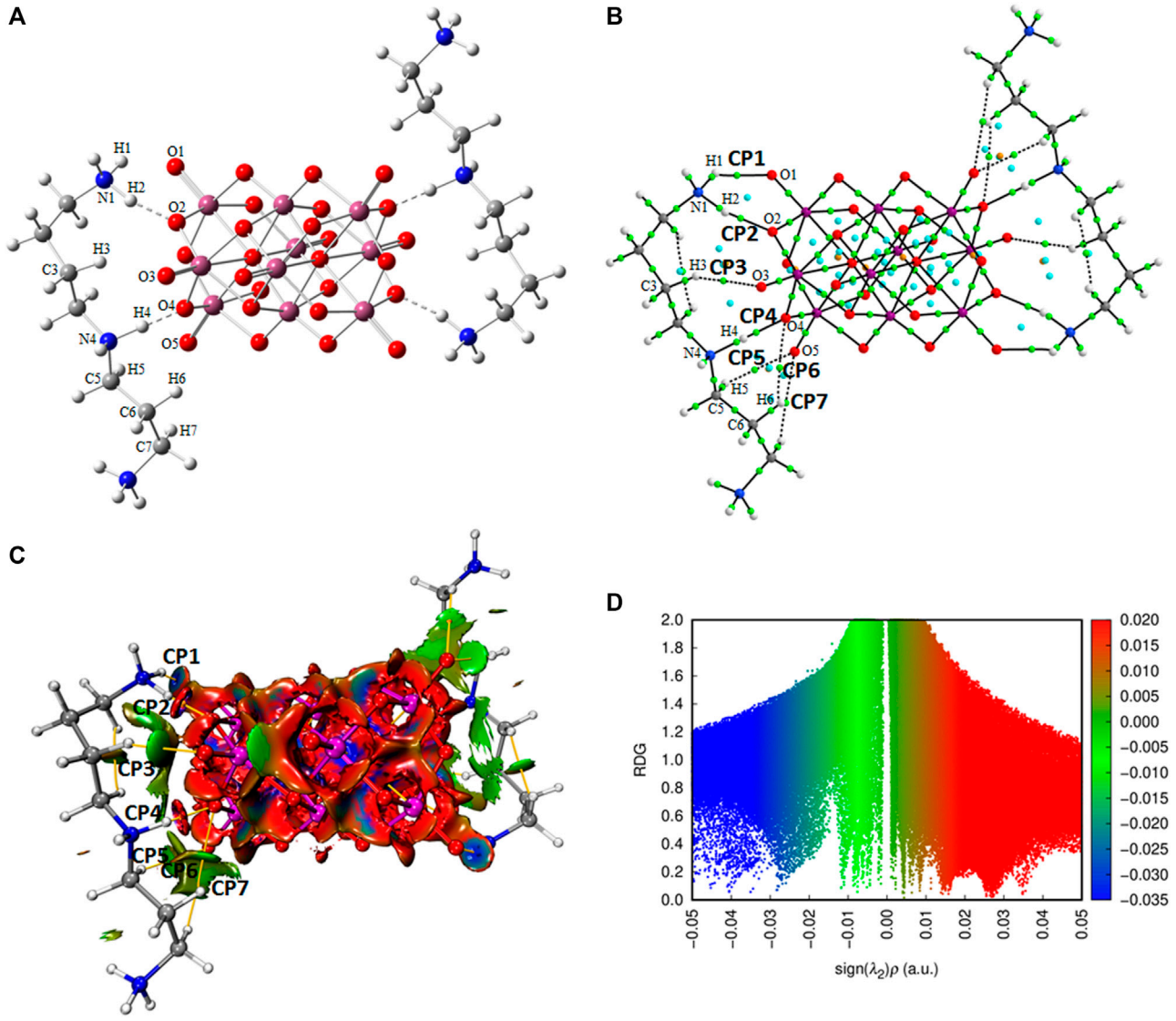

FIGURE 12
(A) Optimized structure of Compound 2 formed by one anion of $[V_{10}O_{28}]^{6-}$ linked by two spermidinium cations; **(B)** Molecular graph showing the main hydrogen bonds between the decavanadate anion and spermidinium cations; **(C)** Non-covalent Interaction (NCI) graph; and **(D)** Reduced Density Gradient (RDG) graph.

systems. The guanidinium cation at the end of the side chain of arginine is a versatile, functional group with unique properties (Arakawa and Timasheff, 1984). Examples of artificial receptors for carboxylates, phosphates, and other oxoanions, such as sulfate or nitrate, have been described (Blondeau et al., 2007). Thus, the guanidinium cation is a small and convenient cation to model the non-covalent interactions of arginine side chains (Makhatadze and Privalov, 1992; Mayr and Schmid, 1993; Makhatadze, 1999; Mason et al., 2004; Schug and Lindner, 2005; Mason et al., 2007; Negi et al., 2023) As for spermidinium, it is also a small polyamine that could serve as a biomimetic model of the lysine side chain. It is a naturally occurring molecule that may be found in plants and semen. It has benefits such as neuroprotection, antiaging, anti-inflammatory, and prevention of tumor cell proliferation. Also, many studies have been related to polyamines and their interaction with other proteins that cause cellular damage (Krasnoslobodtsev et al., 2012). Their role in enzymes (Mishra et al., 2015), beneficial uses in lifespan, helping against aging (Madeo et al., 2018; Nampoothiri et al., 2023), antioxidant effects (Jiang et al., 2023), and ameliorating acute pancreatitis have been described (Shen et al., 2023). All the data about spermidine and other polyamines is directed towards most cancers, health diseases, receptors, Alzheimer's, longevity, antiaging, nutritional, and cognitive function (Jiménez-Gutiérrez et al., 2023; Zimmermann et al., 2023).

Previous combined experimental and theoretical studies dealing with decavanadate decorated with organic ions by our research group (Sánchez-Lara et al., 2018; Sánchez-Lara et al., 2019; García-García et al., 2021; Corona-Motolinia et al., 2022) and another group (Msaadi et al., 2022), indicated the formation of non-covalent interactions of the type hydrogen bonds N–H···O and O–H···O. Complexes of decavanadate with cytosinium and metforminium with a 6:1 ratio of cation-anion were characterized, establishing that the compound with cytosinium

was mainly stabilized by π–π stacking interactions and N–H···O hydrogen bonds. In contrast, the compound with metforminium was stabilized by both hydrogen bonds N–H···O and O–H···O (Sánchez-Lara et al., 2018). The study of the complex of diprotonated decavanadate with 4-dimethylaminopyridinium, with a 4:1 ratio of cation-anion, indicated that hydrogen bonds N–H···O and O–H···O played an essential role in the formation of the supramolecular network highly stabilized by stable rings between anions (Sánchez-Lara et al., 2019). The complex of decavanadate with 2-aminopyrimidinium with a 6:1 ratio of cation-anion showed π–π stacking interactions between 2-aminopyrimidinium cations forming stable rings and cage-like structures stabilizing the complex. The hydrogen bonds N–H···O between decavanadate and 2-aminopyrimidinium were characterized by high interaction energies of 23.02 and 11.26 kcal/mol (García-García et al., 2021), which are similar to the values obtained in this work for guanidinium and spermidinium cations (see Table 6). The complex formed by diprotonated decavanadate anion with VO_2(tris (2-pyridylmethyl)aminium) (VO_2(tpma$^+$)) with a 4:1 ratio of cation-anion showed hydrogen bonds O–H···O with interaction energy of 11.92 kcal/mol, contributing significantly in the formation of the supramolecular structure (Corona-Motolinia et al., 2022). In addition, these complexes have been used to test DNA/RNA interactions using molecular docking analysis, showing good affinity energies (García-García et al., 2021; Corona-Motolinia et al., 2022). Complexes formed by diprotonated decavanadate anion with 3-picolylammonium and 4-fluorobenzyl ammonium with 4:1 ratio of cation-anion showed strong hydrogen bonds N–H···O and O–H···O, and weak non-covalent interactions C–H···O and C–H···F, which were corroborated by NCI-RDG analysis observing the characteristics surfaces for hydrogen bonds for N–H···O interactions between cations with decavanadate, for van der Waals interactions for weak non-covalent interactions, and repulsive interactions between atoms of decavanadate anion (Msaadi et al., 2022), as similarly observed in our Compounds 1 and 2 (see Figures 10C, 11C).

Concerning decavanates as potential anticancer metallodrugs, Zhai et al. published one of the initial reports on decavanadate compounds exhibiting anticancer properties. The molecule $Na_4Co(H_2O)_6$ $[V_{10}O_{28}]\cdot 18H_2O$ demonstrates a more remarkable ability to inhibit the growth of human liver cancer (SMMC-7721) and ovarian cancer (SK-OV-3) cell lines in a laboratory setting compared to the currently utilized antitumoral drug 5-fluorouracil.This substance has shown promising results in reducing the weight of liver tumors in rats in live animal experiments (Zhai et al., 2009). In 2010, Li et al. synthesized two decavanadates containing organic ligands that demonstrated inhibitory effects on human lung development (A549) and murine leukemia (Li et al., 2010). Several other articles discussing the possible anticancer properties of decavanadate compounds have been published (Kioseoglou et al., 2015; Cheng et al., 2018; Gu et al., 2020; Amante et al., 2021; Ksiksi et al., 2021; Louati et al., 2021; Ksiksi et al., 2022a; Aureliano, 2022; Ksiksi et al., 2022b; De Sousa-Coelho et al., 2023; Dridi et al., 2024; Ksiksi et al., 2024). All recent studies point out potential anticancer agents against some cancer cell lines. One of the compounds synthesized in our laboratory has been successfully tested *in vitro* in melanoma cells. (De Sousa-Coelho et al., 2022). The hybrid POV metformin-decavanadate (Metf-V10) showed antiproliferative action at much lower concentrations than metformin alone in UACC62 melanoma cells. It had been previously suggested that V_{10} and V_1 could act through different pathways, and Metf-V10 had increased stability and potentially lower intracellular biotransformation. Recently, guanidinium derivatives have been synthesized with similar purposes (Dumitrescu et al., 2023). Therefore, the compounds reported here will be tested for their anticancer potential.

5 Conclusion

Two decavanadate compounds were synthesized and characterized by different experimental techniques: FTIR, Raman, ^{51}V NMR, thermogravimetric analysis, and monocrystalline X-ray diffraction. Vibrational techniques, especially Raman spectroscopy, are very sensitive and give us helpful information about how the decavanadate cluster interacts with similar side chain terminal groups of the amino acids found in proteins. The absorption band positions in the region of V=O_t bond stretching vibrations (1,200-900 cm^{-1}) will make it possible to determine whether a compound's structure comprises a free anion or is involved in several hydrogen bond interactions. It was found that the cations guanidinium and spermidinium can mostly interact with the decavanadate anion through hydrogen bonds and electrostatic interactions. According to what can be observed in the TGA of the compounds, water molecules act as bridges through hydrogen-bonding interactions with the cluster decavanadate itself or with the organic counterions.

We learned more about the molecular structures, electronic properties, theoretical spectra, and non-covalent interactions between decavanadate ions and their counterions through theoretical DFT calculations. The non-covalent interactions of decavanadate with its organic counterions were also analyzed through the Quantum Theory of Atoms in Molecules (QTAIM), Non-covalent Interaction (NCI), and Reduced Density Gradient (RDG) analyses. Both compounds were highly stabilized by strong hydrogen bond interactions N–H···O and weak non-covalent interactions C–H···O. In addition, the interactions between guanidinium and spermidinium cations and decavanadate anion form several stable rings. This study provides new information on non-covalent intermolecular interactions between decavanadate and lateral chains of arginine and lysine in protein environments. Also, it points out significant differences between V_1 and V_{10} since V_{10} doubles the charge and has a high capacity to form strong hydrogen bonds with amino acid cations. Considering that we could have one pair of electrons in the (μ_3) oxygen and two pairs in the O_t and (μ_2) oxygens, the maximum capacity to form hydrogen bonds is 48 for V_{10}, compared with only 11 for V_1. Therefore, a rich set of possibilities for V_{10} interactions with many proteins could be discovered in the near future.

A better understanding of how V-species interact with proteins, along with the data that has been presented, may serve as the foundation for future research, design, and development of novel, potentially active anticancer agents.

Data availability statement

The original contributions presented in the study are included in the article/Supplementary Material, further inquiries can be directed to the corresponding author/s.

Author contributions

LP-P: Conceptualization, Data curation, Investigation, Writing–original draft, Writing–review and editing. AM: Data curation, Formal Analysis, Methodology, Writing–original draft. AG-G: Data curation, Investigation, Methodology, Writing–original draft. LS-D: Data curation, Formal Analysis, Methodology, Writing–original draft. MM: Data curation, Methodology, Writing–original draft. FM: Data curation, Formal Analysis, Investigation, Methodology, Writing–review and editing. MC: Conceptualization, Data curation, Formal Analysis, Investigation, Methodology, Writing–original draft, Writing–review and editing. EG-V: Conceptualization, Formal Analysis, Funding acquisition, Investigation, Methodology, Supervision, Writing–original draft, Writing–review and editing.

Funding

The author(s) declare that financial support was received for the research, authorship, and/or publication of this article. Projects funded for this research include 100108444-VIEP, 100256733-VIEP (BUAP, Mexico), and the PRODEP Academic Group BUAP-CA-263 (SEP, Mexico).

Acknowledgments

Luis Fernando Paredes-Pérez thanks CONAHCyT (Mexico) for M.Sc. scholarship support number 1024423. MC and FM wish to thank the Laboratorio Nacional de Supercómputo del Sureste de México (LNS-BUAP) and the CONAHCyT network of national laboratories for computer resources and support. The authors thank the Vicerrectoría de Investigación y Estudios de Posgrado (VIEP-BUAP, Mexico) and the PRODEP Academic Group BUAP-CA-263 (SEP, Mexico). We are grateful to Patricia Ruiz Gutierrez and Armando Ramírez Monroy for the FTIR measurements carried out in the Lab. de Química de Coordinación y Organometálica del Centro de Química. Instituto de Ciencias (BUAP, Mexico). We also thank Laboratorio Central IFUAP de la Benemérita Universidad Autónoma de Puebla for Raman spectroscopy measurements.

Conflict of interest

The authors declare that the research was conducted in the absence of any commercial or financial relationships that could be construed as a potential conflict of interest.

Publisher's note

Supplementary material

The Supplementary Material for this article can be found online at: https://www.frontiersin.org/articles/10.3389/fchbi.2024.1451167/full#supplementary-material

References

Adamo, C., and Barone, V. (1999). Toward reliable density functional methods without adjustable parameters: the PBE0 model. *J. Chem. Phys.* 110, 6158–6170. doi:10.1063/1.478522

Amanchi, S. R., and Das, S. K. (2018). A versatile polyoxovanadate in diverse cation matrices: a supramolecular perspective. *Front. Chem.* 6, 469. doi:10.3389/fchem.2018.00469

Amante, C., De Sousa-Coelho, A. L., and Aureliano, M. (2021). Vanadium and melanoma: a systematic review. *Metals* 11 (5), 828. doi:10.3390/met11050828

Arakawa, T., and Timasheff, S. N. (1984). Protein stabilization and destabilization by guanidinium salts. *Biochemistry* 23 (25), 5924–5929. doi:10.1021/bi00320a005

Aureliano, M. (2016). Decavanadate toxicology and pharmacological activities: V10 or V1, both or none? *Oxidative Medicine and Cellular Longevity* 2016, 1–8. doi:10.1155/2016/6103457

Aureliano, M. (2022). The future is bright for polyoxometalates. *Biochem.* 2 (1), 8–26. doi:10.3390/biochem2010002

Aureliano, M., and Crans, D. C. (2009). Decavanadate $(V_{10}O_{28})^{6-}$ and oxovanadates: oxometalates with many biological activities. *J. Inorg. Biochem.* 103 (4), 536–546. doi:10.1016/j.jinorgbio.2008.11.010

Aureliano, M., and Gândara, R. M. (2005). Decavanadate effects in biological systems. *J. Inorg. Biochem.* 99 (5), 979–985. doi:10.1016/j.jinorgbio.2005.02.024

Aureliano, M., Gumerova, N. I., and Rompel, A. (2023). The biological applications of metals and metal complexes. *Metals* 13 (6), 1041. doi:10.3390/met13061041

Aureliano, M., Gumerova, N. I., Sciortino, G., Garribba, E., McLauchlan, C. C., Rompel, A., et al. (2022). Polyoxidovanadates' interactions with proteins: an overview. *Coord. Chem. Rev.* 454, 214344. doi:10.1016/j.ccr.2021.214344

Aureliano, M., Gumerova, N. I., Sciortino, G., Garribba, E., Rompel, A., and Crans, D. C. (2021). Polyoxovanadates with emerging biomedical activities. *Coord. Chem. Rev.* 447, 214143. doi:10.1016/j.ccr.2021.214143

Aureliano, M., Mal, S. S., Fraqueza, G., Sousa-Coelho, A. L. D., Faleiro, M. L., Gumerova, N. I., et al. (2024). "Polyoxovanadates: catalysis, pharmacology, antibacterial and anticancer activities," in *Synthesis and applications in chemistry and materials: volume 11: metal coordination and nanomaterials*, 175–202.

Aureliano, M., and Ohlin, C. A. (2014). Decavanadate *in vitro* and *in vivo* effects: facts and opinions. *J. Inorg. Biochem.* 137, 123–130. doi:10.1016/j.jinorgbio.2014.05.002

Aureliano, M., Ohlin, C. A., Vieira, M. O., Marques, M. P. M., Casey, W. H., and Batista de Carvalho, L. A. E. (2016). Characterization of decavanadate and decaniobate solutions by Raman spectroscopy. *Dalton Trans.* 45 (17), 7391–7399. doi:10.1039/c5dt04176g

Avila, P. F., Ripplinger, T. J., Kemper, D. J., Domine, J. L., and Jordan, C. D. (2019). Features of vibrational and electronic structures of decavanadate revealed by resonance Raman spectroscopy and density functional theory. *J. Phys. Chem. Lett.* 10 (20), 6032–6037. doi:10.1021/acs.jpclett.9b02362

Baran, E. J. (2024). Structural and spectroscopic studies related to vanadium chemistry and biochemistry. *Coord. Chem. Rev.* 502, 215549. doi:10.1016/j.ccr.2023.215549

Barceloux, D. G., and Barceloux, D. (1999). Vanadium. *J. Toxicol. Clin. Toxicol.* 37 (2), 265–278. doi:10.1081/clt-100102425

Barrio, D., and Etcheverry, S. (2010). Potential use of vanadium compounds in therapeutics. *Curr. Med. Chem.* 17 (31), 3632–3642. doi:10.2174/092986710793213805

Bartošová, L., Padělková, Z., Rakovský, E., and Schwendt, P. (2012). Synthesis and crystal structure of two copper (II) complexes with coordinated decavanadate ion. *Polyhedron* 31 (1), 565–569. doi:10.1016/j.poly.2011.10.042

Biçer, E., Dege, N., and Coskun, E. (2017). Synthesis, characterization, and crystal structure of a novel decavanadate salt,$[V_{0.50}\ (H_2O)\ _5]_2[H_2\ (V_{10}O_{28})]\cdot 4(H_2O)$. *J. Chil. Chem. Soc.* 62 (3), 3610–3614. doi:10.4067/s0717-97072017000303610

Bijelic, A., Aureliano, M., and Rompel, A. (2018). The antibacterial activity of polyoxometalates: structures, antibiotic effects and future perspectives. *Chem. Commun.* 54 (10), 1153–1169. doi:10.1039/c7cc07549a

Bijelic, A., Aureliano, M., and Rompel, A. (2019). Polyoxometalates as potential next-generation metallodrugs in the combat against cancer. *Angew. Chem. Int. Ed.* 58 (10), 2980–2999. doi:10.1002/anie.201803868

Blondeau, P., Segura, M., Pérez-Fernández, R., and de Mendoza, J. (2007). Molecular recognition of oxoanions based on guanidinium receptors. *Chem. Soc. Rev.* 36 (2), 198–210. doi:10.1039/b603089k

Bosnjakovic-Pavlovic, N., Prevost, J., and Spasojevic-de Bire, A. (2011). Crystallographic statistical study of decavanadate anion based-structures: toward a prediction of non-covalent interactions. *Cryst. Growth & Des.* 11 (9), 3778–3789. doi:10.1021/cg200236d

Bougie, I., and Bisaillon, M. (2006). Inhibition of a metal-dependent viral RNA triphosphatase by decavanadate. *Biochem. J.* 398 (3), 557–567. doi:10.1042/bj20060198

Budych, M. J. W., Staszak, K., Bajek, A., Pniewski, F., Jastrząb, R., Staszak, M., et al. (2023). The future of polyoxymetalates for biological and chemical apllications. *Coord. Chem. Rev.* 493, 215306. doi:10.1016/j.ccr.2023.215306

Carvalho, F., and Aureliano, M. (2023). Polyoxometalates impact as anticancer agents. *Int. J. Mol. Sci.* 24 (5), 5043. doi:10.3390/ijms24055043

Caswell, L. R. (2003). Andrés del Río, Alexander Von Humboldt, and the twice-discovered element. *Bull. Hist. Chem.* 28 (1), 35.

Chen, K., Dai, G., Liu, S., and Wei, Y. (2023). Reducing obesity and inflammation in mice with organically-derivatized polyoxovanadate clusters. *Chin. Chem. Lett.* 34 (5), 107638. doi:10.1016/j.cclet.2022.06.061

Cheng, M., Li, N., Wang, N., Hu, K., Xiao, Z., Wu, P., et al. (2018). Synthesis, structure and antitumor studies of a novel decavanadate complex with a wavelike two-dimensional network. *Polyhedron* 155, 313–319. doi:10.1016/j.poly.2018.08.052

Contreras-Cadena, D. A., Gómez-Pech, C., Rangel-García, M., Ruiz-Hernández, A., Martinez-Bulit, P., and Barba-Behrens, N. (2014). La importancia del vanadio en los seres vivos. *Educ. Quím.* 25, 245–253. doi:10.1016/s0187-893x(14)70564-6

Corona-Motolinia, N. D., Martínez-Valencia, B., Noriega, L., Sánchez-Gaytán, B. L., Melendez, F. J., García-García, A., et al. (2022). Tris(2-Pyridylmethylamine)$V(O)_2$ complexes as counter ions of diprotonated decavanadate anion: potential antineoplastic activity. *Front. Chem.* 10, 830511. doi:10.3389/fchem.2022.830511

Correia, I., Avecilla, F., Marcão, S., and Costa Pessoa, J. (2004). Structural studies of decavanadate compounds with organic molecules and inorganic ions in their crystal packing. *Inorganica Chim. Acta* 357 (15), 4476–4487. doi:10.1016/j.ica.2004.06.055

Crans, D. C. (1994). Enzyme interactions with labile oxovanadates and other polyoxometalates. *Comments Inorg. Chem.* 16 (1-2), 35–76. doi:10.1080/02603599408035851

Crans, D. C., Henry, L., Cardiff, G., and Posner, B. I. (2019). Developing vanadium as an antidiabetic or anticancer drug: a clinical and historical perspective. *Metall. Ions Life Sci.* 19, 203–230. doi:10.1515/9783110527872-014

Crans, D. C., Mahroof-Tahir, M., Anderson, O. P., and Miller, M. M. (1994). X-ray structure of $(NH_4)_6$(Gly-Gly)$_2V_{10}O_{28}$•$4H_2O$: model studies for polyoxometalate-protein interactions. *Inorg. Chem.* 33 (24), 5586–5590. doi:10.1021/ic00102a036

Crans, D. C., Smee, J. J., Gaidamauskas, E., and Yang, L. (2004). The chemistry and biochemistry of Vanadium and the biological activities exerted by vanadium compounds. *Chem. Rev.* 104 (2), 849–902. doi:10.1021/cr020607t

Casarrubias-Tabarez, B., Rivera-Fernández, N., Rojas-Lemus, M., López-Valdez, N., and Fortoul, T. (2023). Vanadium compounds as antiparasitic agents: An approach to their mechanisms of action. *J. Trace Elem. Med. Bio.* 78, 127201. doi:10.1016/j.jtemb.2023.127201

Crans, D. C., Yang, L., Haase, A., and Yang, X. (2018). Health benefits of Vanadium and its potential as an anticancer agent. *Metall. Ions Life Sci.* 18, 251–279. doi:10.1515/9783110470734-015

CrysAlisPro (2013). Agilent. Available at: https://www.agilent.com/cs/library/usermanuals/Public/CrysAlis_Pro_User_Manual.pdf.

Cuevas, A. O., Castro Ramírez, R., Sánchez García, J. J., López-Sandoval, H., and Barba-Behrens, N. (2012). Química Inorgánica Medicinal: vanadio, platino, oro. *Educ. Quím.* 23 (1), 33–40. doi:10.1016/s0187-893x(17)30095-2

Del Carpio, E., Hernández, L., Ciangherotti, C., Villalobos Coa, V., Jiménez, L., Lubes, V., et al. (2018). Vanadium: history, chemistry, interactions with α-amino acids and potential therapeutic applications. *Coord. Chem. Rev.* 372, 117–140. doi:10.1016/j.ccr.2018.06.002

DeMaster, E. G., and Mitchell, R. A. (1973). Comparison of arsenate and vanadate as inhibitors or uncouplers of mitochondrial and glycolytic energy metabolism. *Biochemistry* 12 (19), 3616–3621. doi:10.1021/bi00743a007

Dennington, R. D. I. I., Keith, T. A., and Millam, J. M. (2016). *GaussView, version 6.0.16*. Shawnee Mission, KS, USA: Semichem Inc.

De Sousa-Coelho, A. L., Aureliano, M., Fraqueza, G., Serrão, G., Gonçalves, J., Sánchez-Lombardo, I., et al. (2022). Decavanadate and metformin-decavanadate effects in human melanoma cells. *J. Inorg. Biochem.* 235, 111915. doi:10.1016/j.jinorgbio.2022.111915

De Sousa-Coelho, A. L., Fraqueza, G., and Aureliano, M. (2023). Repurposing therapeutic drugs complexed to vanadium in cancer. *Pharmaceuticals* 17 (1), 12. doi:10.3390/ph17010012

Diaz, A., Muñoz-Arenas, G., Venegas, B., Vázquez-Roque, R., Flores, G., Guevara, J., et al. (2021). Metforminium decavanadate (MetfDeca) treatment ameliorates hippocampal neurodegeneration and recognition memory in a metabolic syndrome model. *Neurochem. Res.* 46, 1151–1165. doi:10.1007/s11064-021-03250-z

Díaz, A., Vázquez-Roque, R., Carreto-Meneses, K., Moroni-González, D., Moreno-Rodríguez, J. A., and Treviño, S. (2023). Polyoxidovanadates as a pharmacological option against brain aging. *J. Chem. Neuroanat.* 129, 102256. doi:10.1016/j.jchemneu.2023.102256

Dolomanov, O. V., Bourhis, L. J., Gildea, R. J., Howard, J. A., and Puschmann, H. (2009). OLEX2: a complete structure solution, refinement, and analysis program. *J. Appl. Cryst.* 42 (2), 339–341. doi:10.1107/s0021889808042726

Dridi, R., Abdelkafi-Koubaa, Z., Srairi-Abid, N., Socha, B., and Zid, M. F. (2024). One-pot synthesis, structural investigation, antitumor activity, and molecular docking approach of two decavanadate compounds. *J. Inorg. Biochem.* 255, 112533. doi:10.1016/j.jinorgbio.2024.112533

Duan, J., Li, Z., Li, J., Santa-Cruz, A., Sanchez-Martinez, S., Zhang, J., et al. (2018). Structure of full-length human TRPM4. *Proc. Natl. Acad. Sci.* 115 (10), 2377–2382. doi:10.1073/pnas.1722038115

Dumitrescu, A., Maxim, C., Badea, M., Rostas, A. M., Ciorîță, A., Tirsoaga, A., et al. (2023). Decavanadate-bearing guanidine derivatives developed as antimicrobial and antitumor species. *Int. J. Mol. Sci.* 24 (24), 17137. doi:10.3390/ijms242417137

Evangelou, A. M. (2002). Vanadium in cancer treatment. *Crit. Rev. Oncology/Hematology* 42 (3), 249–265. doi:10.1016/s1040-8428(01)00221-9

Evans, H. T. (1966). The molecular structure of the isopoly complex ion, decavanadate $(V_{10}O_{28})^{6-}$. *Inorg. Chem.* 5 (6), 967–977. doi:10.1021/ic50040a004

Ferretti, V. A., and León, I. E. (2022). An overview of Vanadium and cell signaling in potential cancer treatments. *Inorganics* 10 (4), 47. doi:10.3390/inorganics10040047

Frisch, M. J., Trucks, G. W., Schlegel, H. B., Scuseria, G. E., Robb, M. A., Cheeseman, J. R., et al. (2016). *Gaussian 16, revision B.01*. Wallingford, CT, USA: Gaussian Inc.

Frost, R. L., and Palmer, S. J. (2011). Raman spectroscopic study of pascoite $Ca_3V_{10}O_{28}$· $17H_2O$. *Spectrochimica Acta Part A Mol. Biomol. Spectrosc.* 78 (1), 248–252. doi:10.1016/j.saa.2010.10.002

García-García, A., Noriega, L., Meléndez-Bustamante, F. J., Castro, M. E., Sánchez-Gaytán, B. L., Choquesillo-Lazarte, D., et al. (2021). 2-Aminopyrimidinium decavanadate: experimental and theoretical characterization, molecular docking, and potential antineoplastic activity. *Inorganics* 9 (9), 67. doi:10.3390/inorganics9090067

García-García, A., Rojas, S., and Rodríguez-Diéguez, A. (2023). Therapy and diagnosis of Alzheimer's disease: from discrete metal complexes to metal– organic frameworks. *J. Mater. Chem.* 11 (30), 7024–7040. doi:10.1039/D3TB00427A

Ghosh, M., Sorsche, D., Binte Ahmed, R., and Anjass, M. (2023). Stabilizing decavanadate cluster as electrode material in sodium and lithium-ion batteries. *ChemSusChem* 16 (24), e202300631. doi:10.1002/cssc.202300631

Gonzalez-Cano, S. I., Flores, G., Guevara, J., Morales-Medina, J. C., Treviño, S., and Diaz, A. (2023). Polyoxidovanadates a new therapeutic alternative for neurodegenerative and aging diseases. *Neural Regen. Res.* 19, 571–577. doi:10.4103/1673-5374.380877

Gu, Y., Li, Q., Huang, Y., Zhu, Y., Wei, Y., and Ruhlmann, L. (2020). Polyoxovanadate-iodobodipy supramolecular assemblies: new agents for high efficiency cancer photochemotherapy. *Chem. Commun.* 56, 2869–2872. doi:10.1039/c9cc09944a

Guilherme, L. R., Massabni, A. C., Dametto, A. C., de Souza Corrêa, R., and de Araujo, A. S. (2010). Synthesis, infrared spectroscopy, and crystal structure determination of a new decavanadate. *J. Chem. Crystallogr.* 40, 897–901. doi:10.1007/s10870-010-9759-x

Gumerova, N. I., and Rompel, A. (2018). Synthesis, structures, and applications of electron-rich polyoxometalates. *Nat. Rev. Chem.* 2 (2), 0112. doi:10.1038/s41570-018-0112

Gumerova, N. I., and Rompel, A. (2020). Polyoxometalates in solution: speciation under spotlight. *Chem. Soc. Rev.* 49 (21), 7568–7601. doi:10.1039/d0cs00392a

Hartung, S., Bucher, N., Chen, H. Y., Al-Oweini, R., Sreejith, S., Borah, P., et al. (2015). Vanadium-based polyoxometalate as new material for sodium-ion battery anodes. *J. Power Sources* 288, 270–277. doi:10.1016/j.jpowsour.2015.04.009

Hay, P. J., and Wadt, W. R. (1985). *Ab initio* effective core potentials for molecular calculations. Potentials for the transition metal atoms Sc to Hg. *J. Chem. Phys.* 82, 270–283. doi:10.1063/1.448799

Humphrey, W., Dalke, A., and Schulten, K. (1996). VMD-visual molecular dynamics. *J. Mol. Graph.* 14, 33–38. doi:10.1016/0263-7855(96)00018-5

Jiang, D., Guo, Y., Niu, C., Long, S., Jiang, Y., Wang, Z., et al. (2023). Exploration of the antioxidant effect of spermidine on the ovary and screening and identification of differentially expressed proteins. *Int. J. Mol. Sci.* 24 (6), 5793. doi:10.3390/ijms24065793

Jimenez Gutierrez, G. E., Borbolla Jiménez, F. V., Muñoz, L. G., Tapia Guerrero, Y. S., Murillo Melo, N. M., Cristóbal-Luna, J. M., et al. (2023). The molecular role of polyamines in age-related diseases: an update. *Int. J. Mol. Sci.* 24 (22), 16469. doi:10.3390/ijms242216469

Keith, T. A. (2019). *TK gristmill software*. Overland Park, KS, USA: AIMAll. Version 19.02. 13.

Kioseoglou, E., Petanidis, S., Gabriel, C., and Salifoglou, A. (2015). The chemistry and biology of vanadium compounds in cancer therapeutics. *Coord. Chem. Rev.* 301-302, 87–105. doi:10.1016/j.ccr.2015.03.010

Krasnoslobodtsev, A. V., Peng, J., Asiago, J. M., Hindupur, J., Rochet, J. C., and Lyubchenko, Y. L. (2012). Effect of spermidine on misfolding and interactions of alpha-synuclein. *PloS one* 7 (5), e38099. doi:10.1371/journal.pone.0038099

Krivosudský, L., Roller, A., and Rompel, A. (2019). Tuning the interactions of decavanadate with thaumatin, lysozyme, proteinase K, and human serum proteins by its coordination to a pentaaquacobalt (II) complex cation. *New J. Chem.* 43 (45), 17863–17871. doi:10.1039/c9nj02495f

Ksiksi, R., Abdelkafi-Koubaa, Z., Mlayah-Bellalouna, S., Aissaoui, D., Marrakchi, N., Srairi-Abid, N., et al. (2021). Synthesis, structural characterization, and antitumoral activity of $(NH_4)_4Li_2V_{10}O_{28}$. $10H_2O$ compound. *J. Mol. Struct.* 1229, 129492. doi:10.1016/j.molstruc.2020.129492

Ksiksi, R., Bellalouna, S. M., Abdelkafi-Koubaa, Z., Aissa, T., Marrakchi, N., Srairi-Abid, N., et al. (2024). $(C_4N_2H_7)_6(C_4N_2H_6)_2V_{10}O_{28}$ decavanadate compound: synthesis, chemical characterization, and assessment of antitumor potential. *Russ. J. Inorg. Chem.*, 1–9. doi:10.1134/s0036023624600618

Ksiksi, R., Essid, A., Kouka, S., Boujelbane, F., Daoudi, M., Srairi-Abid, N., et al. (2022a). Synthesis and characterization of a tetra-(benzylammonium) dihydrogen decavanadate dihydrate compound inhibiting MDA-MB-231 human breast cancer cells proliferation and migration. *J. Mol. Struct.* 1250, 131929. doi:10.1016/j.molstruc.2021.131929

Ksiksi, R., Essid, A., Kouka, S., Boujelbane, F., Daoudi, M., Srairi-Abid, N., et al. (2022b). Synthesis and characterization of a tetra-(benzylammonium) dihydrogen decavanadate dihydrate compound inhibiting MDA-MB-231 human breast cancer cells proliferation and migration. *J. Mol. Struct.* 1250, 131929. doi:10.1016/j.molstruc.2021.131929

Li, Y.-T., Zhu, C.-Y., Wu, Z.-Y., Jiang, M., and Yan, C.-W. (2010). Synthesis, crystal structures and anticancer activities of two decavanadate compounds. *Transit. Metal. Chem.* 35, 597–603. doi:10.1007/s11243-010-9369-7

Louati, M., Ksiksi, R., Elbini-Dhouib, I., Mlayah-Bellalouna, S., Doghri, R., Srairi-Abid, N., et al. (2021). Synthesis, structure, and characterization of a novel decavanadate, $Mg(H_2O)_6(C_4N_2H_7)_4V_{10}O_{28}$ $4H_2O$. *J. Mol. Struct.* 1242, 130711. doi:10.1016/j.molstruc.2021.130711

Lu, T., and Chen, F. (2012). Multiwfn: a multifunctional wavefunction analyzer. *J. Comput. Chem.* 33, 580–592. doi:10.1002/jcc.22885

Madeo, F., Eisenberg, T., Pietrocola, F., and Kroemer, G. (2018). Spermidine in health and disease. *Science* 359 (6374), eaan2788. doi:10.1126/science.aan2788

Makhatadze, G. I. (1999). Thermodynamics of protein interactions with urea and guanidinium hydrochloride. *J. Phys. Chem. B* 103 (23), 4781–4785. doi:10.1021/jp990413q

Makhatadze, G. I., and Privalov, P. L. (1992). Protein interactions with urea and guanidinium chloride: a calorimetric study. *J. Mol. Biol.* 226 (2), 491–505. doi:10.1016/0022-2836(92)90963-k

Manganaro, J., Levina, A., Lay, P. A., and Crans, D. C. (2022). Potential applications of vanadium-based anticancer drugs for intratumoral injections. *Med. Sci. Forum* 11 (1), 10. MDPI. doi:10.3390/BiTaP-12783

Mason, P. E., Brady, J. W., Neilson, G. W., and Dempsey, C. E. (2007). The interaction of guanidinium ions with a model peptide. *Biophysical J.* 93 (1), L04–L06. doi:10.1529/biophysj.107.108290

Mason, P. E., Neilson, G. W., Enderby, J. E., Saboungi, M. L., Dempsey, C. E., MacKerell, A. D., Jr, et al. (2004). The structure of aqueous guanidinium chloride solutions. *J. Am. Chem. Soc.* 126 (37), 11462–11470. doi:10.1021/ja040034x

Mayr, L. M., and Schmid, F. X. (1993). Stabilization of a protein by guanidinium chloride. *Biochemistry* 32 (31), 7994–7998. doi:10.1021/bi00082a021

Mishra, A. K., Agnihotri, P., Srivastava, V. K., and Pratap, J. V. (2015). Novel protein-protein interaction between spermidine synthase and S-adenosylmethionine decarboxylase from Leishmania donovani. *Biochem. Biophysical Res. Commun.* 456 (2), 637–642. doi:10.1016/j.bbrc.2014.12.008

Missina, J. M., Gavinho, B., Postal, K., Santana, F. S., Valdameri, G., De Souza, E. M., et al. (2018). Effects of decavanadate salts with organic and inorganic cations on *Escherichia coli*, Giardia intestinalis, and Vero cells. *Inorg. Chem.* 57 (19), 11930–11941. doi:10.1021/acs.inorgchem.8b01298

Missina, J. M., Leme, L. B., Postal, K., Santana, F. S., Hughes, D. L., De Sá, E. L., et al. (2020). Accessing decavanadate chemistry with tris (hydroxymethyl) aminomethane and evaluation of methylene blue bleaching. *Polyhedron* 180, 114414. doi:10.1016/j.poly.2020.114414

Mizuno, N., and Kamata, K. (2011). Catalytic oxidation of hydrocarbons with hydrogen peroxide by vanadium-based polyoxometalates. *Coord. Chem. Rev.* 255 (19-20), 2358–2370. doi:10.1016/j.ccr.2011.01.041

Moskalyk, R. R., and Alfantazi, A. M. (2003). Processing of vanadium: a review. *Miner. Eng.* 16 (9), 793–805. doi:10.1016/s0892-6875(03)00213-9

Msaadi, I., Rayes, A., Benito, M., Issaoui, N., Molins, E., and Ayed, B. (2022). A combined experimental and theoretical studies of two new decavanadates: $(C_6N_2H_9)_4[H_2V_{10}O_{28}]\cdot 4H_2O$ and $(C_7H_9NF)_4[H_2V_{10}O_{28}]\cdot 2H_2O$. *J. Mol. Struct.* 1262, 133085. doi:10.1016/j.molstruc.2022.133085

Nampoothiri, M., Kolathur, K. K., Sankhe, R., and Satarker, S. (2023). "Spermidine, an autophagy inducer, as a therapeutic antiaging strategy," in *Emerging antiaging strategies* (Singapore: Springer Nature Singapore), 135–153.

Negi, I., Jangra, R., Gharu, A., Trant, J. F., and Sharma, P. (2023). Guanidinium–amino acid hydrogen-bonding interactions in protein crystal structures: implications for guanidinium-induced protein denaturation. *Phys. Chem. Chem. Phys.* 25 (1), 857–869. doi:10.1039/d2cp04943k

Omri, I., Mhiri, T., and Graia, M. (2015). Novel decavanadate cluster complex $(HImz)_{12}(V_{10}O_{28})_2\cdot$ $3H_2O$: synthesis, characterization, crystal structure, optical and thermal properties. *J. Mol. Struct.* 1098, 324–331. doi:10.1016/j.molstruc.2015.06.011

Parr, R. G., and Yang, W. (1989). "Density-functional theory of atoms and molecules," in *International series of monograph on chemistry-16* (New York, NY, USA: Oxford University Press).

Patel, N., Prajapati, A. K., Jadeja, R. N., Patel, R. N., Patel, S. K., Gupta, V. K., et al. (2019). Model investigations for vanadium-protein interactions: synthesis, characterization and antidiabetic properties. *Inorganica Chim. Acta* 493, 20–28. doi:10.1016/j.ica.2019.04.050

Pessoa, J. C., Etcheverry, S., and Gambino, D. (2015). Vanadium compounds in medicine. *Coord. Chem. Rev.* 301-302, 24–48. doi:10.1016/j.ccr.2014.12.002

Pessoa, J. C., Santos, M. F., Correia, I., Sanna, D., Sciortino, G., and Garribba, E. (2021). Binding of vanadium ions and complexes to proteins and enzymes in aqueous solution. *Coord. Chem. Rev.* 449, 214192. doi:10.1016/j.ccr.2021.214192

Pisano, M., Arru, C., Serra, M., Galleri, G., Sanna, D., Garribba, E., et al. (2019). Antiproliferative activity of vanadium compounds: effects on the major malignant melanoma molecular pathways. *Metallomics* 11 (10), 1687–1699. doi:10.1039/c9mt00174c

Pope, M. T., and Müller, A. (1991). Polyoxometalate chemistry: an old field with new dimensions in several disciplines. *Angew. Chem. Int. Ed. Engl.* 30 (1), 34–48. doi:10.1002/anie.199100341

Rakovský, E., Žúrková, Ľ., and Marek, J. (2002). Synthesis, crystal structure, and IR spectroscopic characterization of 1, 6-hexanediammonium dihydrogendecavanadate. *Monatsh. Chem.* 133, 277–283. doi:10.1007/s007060200005

Rao, A. S., Arumuganathan, T., Shivaiah, V., and Das, S. K. (2011). Polyoxometalates: toward new materials. *J. Chem. Sci.* 123, 229–239. doi:10.1007/s12039-011-0115-2

Rehder, D. (2008). *Bioinorganic vanadium chemistry*. John Wiley and Sons.

Rehder, D. (2013a). The future of/for Vanadium. *Dalton Trans.* 42 (33), 11749–11761. doi:10.1039/c3dt50457c

Rehder, D. (2013b). Vanadium. Its role for humans. *Metal Ions Life Sci.* 13, 139–169. doi:10.1007/978-94-007-7500-8_5

Rehder, D. (2015b). The role of Vanadium in biology. *Metallomics* 7 (5), 730–742. doi:10.1039/c4mt00304g

Rehder, D. (2015a). The (biological) speciation of vanadate (V) as revealed by ^{51}V NMR: a tribute on Lage Pettersson and his work. *J. Inorg. Biochem.* 147, 25–31. doi:10.1016/j.jinorgbio.2014.12.014

Rehder, D. (2017). Implications of vanadium in technical applications and pharmaceutical issues. *Inorganica Chim. Acta* 455, 378–389. doi:10.1016/j.ica.2016.06.021

Rehder, D. (2023). Vanadium in biological systems and medicinal applications. *Inorganica Chim. Acta* 549, 121387. doi:10.1016/j.ica.2023.121387

Sánchez-Lara, E. (2020). El vanadio: desde su descubrimiento hasta su papel en la vida. *Educación química* 31 (4), 9–20. doi:10.22201/fq.18708404e.2020.4.75702

Sánchez-Lara, E., Martínez-Valencia, B., Corona-Motolinia, N. D., Sanchez-Gaytan, B. L., Castro, M. E., Bernès, S., et al. (2019). A one-dimensional supramolecular chain based on $[H_2V_{10}O_{28}]^{4-}$ units decorated with 4-dimethylaminopyridinium ions: an experimental and theoretical characterization. *New J. Chem.* 43 (45), 17746–17755. doi:10.1039/c9nj02097g

Sánchez-Lara, E., Pérez-Benítez, A., Treviño, S., Mendoza, A., Meléndez, F. J., Sánchez-Mora, E., et al. (2016). Synthesis and 3D network architecture of 1-and 16-hydrated salts of 4-dimethylaminopyridinium decavanadate $(DMAPH)_6[V_{10}O_{28}]\cdot nH_2O$. *Crystals* 6 (6), 65. doi:10.3390/cryst6060065

Sánchez-Lara, E., Sánchez-Lombardo, I., Pérez-Benítez, A., Mendoza, Á., Flores-Álamo, M., and Vergara, E. G. (2015). A new dicationic ring [(water) 6–(ammonium) 2] acts as a building block for a supramolecular 3D assembly of decavanadate clusters and 4-(N, N-dimethylamino) pyridinium ions. *J. Clust. Sci.* 26, 901–912. doi:10.1007/s10876-014-0779-0

Sánchez-Lara, E., Treviño, S., Sánchez-Gaytán, B. L., Sánchez-Mora, E., Eugenia Castro, M., Meléndez-Bustamante, F. J., et al. (2018). Decavanadate salts of cytosine and metformin: a combined experimental-theoretical study of potential metallodrugs against diabetes and cancer. *Front. Chem.* 6, 402. doi:10.3389/fchem.2018.00402

Sánchez-Lombardo, I., Sánchez-Lara, E., Pérez-Benítez, A., Mendoza, Á., Bernès, S., and González-Vergara, E. (2014). Synthesis of metforminium (2+) decavanadates–crystal structures and solid-state characterization. *Eur. J. Inorg. Chem.* 2014 (27), 4581–4588. doi:10.1002/ejic.201402277

Schug, K. A., and Lindner, W. (2005). Non-covalent binding between guanidinium and anionic groups: focus on biological and synthetic-based arginine/guanidinium interactions with phosph [on] ate and sulf [on] ate residues. *Chem. Rev.* 105 (1), 67–114. doi:10.1021/cr040603j

Ścibior, A., Aureliano, M., and Llopis, J. (2024). Emerging topics in metal complexes: pharmacological activity. *Int. J. Mol. Sci.* 25 (9), 4982. doi:10.3390/ijms25094982

Sheldrick, G. M. (2015). SHELXT–Integrated space-group and crystal-structure determination. *Acta Crystallogr. Sect. A Found. Adv.* 71 (1), 3–8. doi:10.1107/s2053273314026370

Shen, Y., Duan, H., Yuan, L., Asikaer, A., Liu, Y., Zhang, R., et al. (2023). Computational biology-based study of the molecular mechanism of spermidine amelioration of acute pancreatitis. *Mol. Divers.*, 1–19. doi:10.1007/s11030-023-10698-4

Singh, A., and Singh, P. (2021). A linguistic study of chemical terminology. *Webology* 18 (2). *(ISSN: 1735-188X)*.

Siva, V., Kumar, S. S., Shameem, A., Raja, M., Athimoolam, S., and Bahadur, S. A. (2017). Structural, spectral, quantum chemical and thermal studies on a new NLO crystal: guanidinium cinnamate. *J. Mat. Sci. Mat. Electron.* 28, 12484–12496. doi:10.1007/s10854-017-7070-8

Stephan, H., Kubeil, M., Emmerling, F., and Müller, C. E. (2013). Polyoxometalates as versatile enzyme inhibitors. *Eur. J. Inorg. Chem.* 2013 (10-11), 1585–1594. doi:10.1002/ejic.201201224

Todorović, M. R., Mioč, U. B., Holclajtner-Antunović, I., and Šegan, D. (2005). Synthesis and characterization of ammonium Decavanadate (V). *Mater. Sci. Forum* 494, 351–356. *Trans. Tech. Publ. Ltd.* doi:10.4028/0-87849-971-7.351

Tomasi, J., Mennucci, B., and Cammi, R. (2005). Quantum mechanical continuum solvation models. *Chem. Rev.* 105, 2999–3094. doi:10.1021/cr9904009

Treviño, S., Díaz, A., Sánchez-Lara, E., Sanchez-Gaytan, B. L., Perez-Aguilar, J. M., and González-Vergara, E. (2019). Vanadium in biological action: chemical, pharmacological aspects, and metabolic implications in diabetes mellitus. *Biol. Trace Elem. Res.* 188, 68–98. doi:10.1007/s12011-018-1540-6

Treviño, S., Velázquez-Vázquez, D., Sánchez-Lara, E., Diaz-Fonseca, A., Flores-Hernandez, J. Á., Pérez-Benítez, A., et al. (2016). Metforminium decavanadate as a potential metallopharmaceutical drug for the treatment of diabetes mellitus. *Oxidative Med. Cell. Longev.* 2016 (1), 1–14. doi:10.1155/2016/6058705

Tsiani, E., and Fantus, I. G. (1997). Vanadium compounds: biological actions and potential as pharmacological agents. *Trends Endocrinol. Metabolism* 8 (2), 51–58. doi:10.1016/s1043-2760(96)00262-7

Van Cleave, C., and Crans, D. C. (2019). The first-row transition metals in the periodic table of medicine. *Inorganics* 7 (9), 111. doi:10.3390/inorganics7090111

Venkataraman, B. V., Ravishankar, H. N., Rao, A. V., Kalyani, P., Sharada, G., Namboodiri, K., et al. (1997). Decavanadate possesses alpha-adrenergic agonist activity and a structural motif common with trans-beta form of noradrenaline. *Mol. Cell. Biochem.* 169, 27–36. doi:10.1023/a:1006882408983

Wang, X., Liu, H., Xu, X., and You, X. (1993). The crystal structure of the addition compound of decavanadate and guanidine. *Polyhedron* 12 (1), 77–81. doi:10.1016/s0277-5387(00)87056-4

Weigend, F., and Ahlrichs, R. (2005). Balanced basis sets of split valence, triple zeta valence and quadruple zeta valence quality for H to Rn: design and assessment of accuracy. *Phys. Chem. Chem. Phys.* 7, 3297–3305. doi:10.1039/b508541a

Wery, A. S., Gutierrez-Zorrila, J. M., Luque, A., Roman, P., and Martinez-Ripoll, M. (1996). Influence of protonation on crystal packing and thermal behaviour of tert-butylammonium decavanadates. *Polyhedron* 15 (24), 4555–4564. doi:10.1016/0277-5387(96)00186-6

Zhai, F., Wang, X., Li, D., Zhang, H., Li, R., and Song, L. (2009). Synthesis and biological evaluation of decavanadate $Na_4Co(H_2O)_6V_{10}O_{28}{\cdot}18H_2O$. *Biomed. Pharmacother.* 63, 51–55. doi:10.1016/j.biopha.2008.01.006

Zhao, M., Chen, X., Chi, G., Shuai, D., Wang, L., Chen, B., et al. (2020). Research progress on the inhibition of enzymes by polyoxometalates. *Inorg. Chem. Front.* 7 (22), 4320–4332. doi:10.1039/d0qi00860e

Zimmermann, A., Hofer, S. J., and Madeo, F. (2023). Molecular targets of spermidine: implications for cancer suppression. *Cell Stress* 7 (7), 50–58. doi:10.15698/cst2023.07.281